A high-order discontinuous Galerkin approach to the elasto-acoustic problem*

Paola F. Antonietti[a], Francesco Bonaldi[a,*], Ilario Mazzieri[a]

[a] *MOX, Dipartimento di Matematica, Politecnico di Milano*
Piazza Leonardo da Vinci 32, 20133 Milano, Italy

Abstract

We address the spatial discretization of an evolution problem arising from the coupling of elastic and acoustic wave propagation phenomena by employing a discontinuous Galerkin scheme on polygonal and polyhedral meshes. The coupled nature of the problem is ascribed to suitable transmission conditions imposed at the interface between the solid (elastic) and fluid (acoustic) domains. We state and prove a well-posedness result for the strong formulation of the problem, present a stability analysis for the semi-discrete formulation, and finally prove an *a priori hp*-version error estimate for the resulting formulation in a suitable (mesh-dependent) energy norm. We also discuss the time integration scheme employed to obtain the fully discrete system. The convergence results are validated by numerical experiments carried out in a two-dimensional setting.

Keywords: discontinuous Galerkin methods, elastodynamics, acoustics, wave propagation, polygonal and polyhedral grids
2010 MSC: 65M12, 65M60

1. Introduction

This work is devoted to the development and analysis of a discontinuous Galerkin (dG) method [1, 2, 3, 4] on polygonal and polyhedral grids for an evolution problem modeling coupled (visco)elastic-acoustic wave propagation. Coupled elasto-acoustic wave propagation arises in several scientific and engineering contexts. In a geophysics framework, on which we focus here, a first example one can think of is given by seismic events occurring near coastal environments; another relevant situation where such a problem plays a major role is the detection of underground cavities [5, 6, 7]. Other contexts in which this problem plays a major role are the modeling of sensing or actuation devices immersed in an acoustic fluid [8], as well as medical ultrasonics [9].

From the numerical viewpoint, a discretization scheme employed for simulating seismic wave propagation scenarios has to satisfy the following requirements: *accuracy*, *geometric flexibility*,

*This work has been supported by SIR Research Grant no. RBSI14VTOS funded by MIUR – Italian Ministry of Education, Universities, and Research, and by "National Group of Scientific Computing" (GNCS-INdAM).

*Corresponding author.
Email addresses: paola.antonietti@polimi.it (Paola F. Antonietti), francesco.bonaldi@polimi.it (Francesco Bonaldi), ilario.mazzieri@polimi.it (Ilario Mazzieri)

and *scalability*. To be *accurate*, the numerical method must keep dissipative and dispersive errors low. *Geometric flexibility* is necessary since the computational domain usually features complicated geometrical shapes as well as sharp discontinuities of mechanical properties. Finally, ground-motion scenarios are typically characterized by domains whose dimension, ranging from hundreds to thousands square kilometers, is very large compared with the wavelengths of interest. This typically leads to a discrete problem featuring several millions of unknowns. As a consequence, parallel algorithms must be *scalable* in order to efficiently exploit high performance computers.

In particular, given the underlying complex geometry one has to deal with, considering a conforming triangulation would therefore be computationally very expensive. We are thus led to consider a space discretization method capable to reproduce the geometrical constraints under consideration to a reasonable extent of accuracy, without being at the same time too much demanding. Such a discretization is then performed using general polygonal or polyhedral (briefly, *polytopic*) elements, with no restriction on the number of faces each element can possess, and possibly allowing for face degeneration in mesh refinement. The dG method has been recently proven to successfully support polygonal/polyhedral meshes: we refer the reader, e.g., to [10, 11, 12, 13, 14, 15, 16, 17, 18], as well as to the comprehensive research monograph by Cangiani *et al.* [19]. Because of their local nature, dG methods are particularly suited to treat highly heterogeneous and soil-structure interaction problems, where local refinements are needed to resolve the different spatial scales, as well as to satisfy the above-mentioned accuracy and scalability requirements for a numerical scheme that is well-suited for wave propagation phenomena. In addition to the dG method, several other methods are capable to support polytopic meshes, such as the Polygonal Finite Element method [20, 21, 22, 23], the Mimetic Finite Difference method [24, 25, 26, 27, 28], the Virtual Element method [29, 30, 31, 32, 33], the Hybridizable Discontinuous Galerkin method [34, 35, 36], and the Hybrid High-Order method [37, 38, 39].

An elasto-acoustic coupling typically occurs in the following framework: a domain made up by two subdomains, one occupied by a solid (elastic) body, the other by a fluid (acoustic) one, with suitable transmission conditions imposed at the interface between the two. The aim of such conditions is to account for the following physical properties: (i) the normal component of the velocity field is continuous at the interface; (ii) a pressure load is exerted by the fluid body on the solid one through the interface. In this paper, the unknowns of the problem are the displacement field in the solid domain and the acoustic potential in the fluid domain; the latter, say φ, is defined in terms of the acoustic velocity field $\mathbf{v}_a$ in such a way that $\mathbf{v}_a = -\boldsymbol{\nabla}\varphi$. However, other formulations are possible; for instance, one can consider a pressure-based formulation in the acoustic subdomain [9], or a displacement-based formulation in both subdomains [40].

In a geophysics context, when a seismic event occurs, both *pressure* (P) and *shear* (S) waves are generated. However, only P-waves (i.e., whose direction of propagation is aligned with the displacement of the medium) are able to travel through both solid and fluid bodies, unlike S-waves (i.e., whose direction of propagation is orthogonal to the displacement of the medium), which can travel only through solids. This explains the reason for considering the first interface condition. On the other hand, the second one accounts for the fact that an acoustic wave propagating in a fluid domain of density ρ_a gives rise to an *acoustic pressure* field of magnitude $\rho_a|\dot{\varphi}|$, $\dot{\varphi}$ denoting the first time derivative of the acoustic potential.

Mathematical and numerical aspects of the elasto-acoustic coupling have been the subject of an extremely broad literature. We give hereinafter a brief overview of some of the research

works carried out so far in this field.

Barucq *et al.* [41] have characterized the Fréchet differentiability of the elasto-acoustic field with respect to Lipschitz-continuous deformation of the shape of an elastic scatterer. The same authors [42] have also proposed a dG method for computing the scattered field from an elastic bounded object immersed in an infinite homogeneous fluid medium, employing high-order polynomial-shape functions to address the high-frequency propagation regime, and curved boundary edges to provide an accurate representation of the fluid-structure interface. Bermúdez *et al.* [40] have solved an interior elasto-acoustic problem in a three-dimensional setting, employing a displacement-based formulation on both the fluid and the solid domains, and a discretization consisting of linear tetrahedral finite elements for the solid and Raviart–Thomas elements of lowest order for the fluid; a further unknown is introduced on the interface between solid and fluid to impose the transmission conditions. Brunner *et al.* [43] have treated the case of thin structures and dense fluids; the structural part is modeled with the finite element method, and the exterior acoustic problem is efficiently modeled with the Galerkin boundary element method. De Basabe and Sen [44] have compared Finite Difference and Spectral Element methods for elastic wave propagation in media with a fluid-solid interface. Fischer and Gaul [45] have proposed a coupling algorithm based on Lagrange multipliers for the simulation of structure-acoustic interaction; finite plate elements are coupled with a Galerkin boundary element formulation of the acoustic domain, and the interface pressure is interpolated as a Lagrange multiplier, thereby allowing for coupling non-matching grids. Flemisch *et al.* [8] have considered a numerical scheme based on two independently generated grids on the elastic and acoustic domains, thereby allowing as much flexibility as possible, given that the computational grid in one subdomain can in general be considerably coarser than in the other subdomain. As a result, non-conforming grids appear at the interface of the two subdomains. Mandel [46] has proposed a parallel iterative method for the solution of the linear equations resulting from the finite element discretization of the coupled fluid-solid systems in fluid pressure and solid displacement formulation, in harmonic regime. Mönköla [47] has examined the accuracy and efficiency of the numerical solution based on high-order discretizations, in the case of transient regime. Spatial discretization is performed by the Spectral Element method, and three different schemes are compared for time discretization. Péron [48] has presented equivalent conditions and asymptotic models for the diffraction problem of elastic and acoustic waves in a solid medium surrounded by a thin layer of fluid medium in harmonic regime. Wilcox *et al.* [49] studied a high-order Discontinuous Galerkin scheme for the three-dimensional problem based on a velocity-strain formulation, allowing for the solution of the acoustic and elastic wave equations within the same unified framework, based on a first-order system of hyperbolic equations. Other noteworthy references in this field are [50, 51, 52, 53, 54, 55, 56, 57, 58].

At the best of our knowledge, in all of the aforementioned works a well-posedness result for the mathematical formulation of the coupled problem cannot be found. In this work, the proof of existence and uniqueness for a strong solution is accomplished in a semigroup framework, by resorting to the Hille–Yosida theorem [59, Chap. 7]. Notice that a similar abstract setting wherein semigroup theory on Hilbert spaces can be invoked, was employed in [60]; here, the problem of acoustic waves scattered by a piezoelectric solid is investigated.

The rest of the paper is organized as follows. In Section 2 we establish the notation employed throughout the paper. In Section 3 we give the formulation of the problem and prove the existence and uniqueness of the solution under suitable hypotheses on source terms and initial values. In

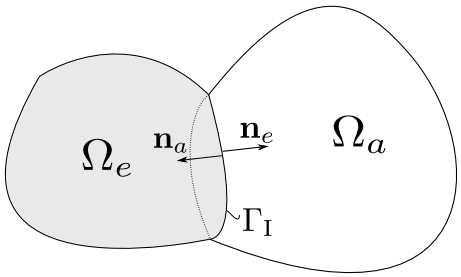

Figure 1: Computational domain.

Section 4 we introduce the discrete setting, with particular reference to the assumptions on the underlying polytopic mesh. In Section 5 we present the formulation of the semi-discrete problem. In Section 6 we state a stability result for the semi-discrete formulation in a suitable (mesh-dependent) energy norm. In Section 7, we present *hp*-convergence results (with h and p denoting, as usual, the meshsize and the polynomial degree, respectively) for the error in the energy norm. In Section 8 we discuss the fully discrete formulation. In Section 9, we present some numerical experiments carried out in a two-dimensional setting to validate the theoretical results for benchmark test cases. In Section 10, we simulate two examples of physical interest: namely, the effects of an acoustic point source near an elastic medium, and the effects of an elastic point source in the presence of acoustic cavities included in the elastic domain. Finally, in Section 11 we draw some conclusions. The proofs of the main theoretical results, contained in Sections 3, 6, and 7, as well as the statements and proofs of two technical lemmas, are postponed to Appendix A.

2. General notation

In what follows, scalar fields are represented by lightface letters, vector fields by boldface roman letters, and second-order tensor fields by boldface greek letters. We let $\Omega \subset \mathbb{R}^d$, $d \in \{2, 3\}$, denote an open bounded domain with Lipschitz boundary, given by the union of two open disjoint bounded convex subdomains Ω_e and Ω_a representing an elastic and an acoustic domain, respectively (cf. Figure 1). We denote by $\Gamma_{\mathrm{I}} = \partial\Omega_e \cap \partial\Omega_a$ the *interface* between the two domains, also of Lipschitz regularity and with strictly positive surface measure. We assume that the following partitions hold: $\partial\Omega_e = \Gamma_{eD} \cup \Gamma_{\mathrm{I}}$ and $\partial\Omega_a = \Gamma_{aD} \cup \Gamma_{\mathrm{I}}$, where Γ_{eD} and Γ_{aD} also have strictly positive surface measure, and $\Gamma_{eD} \cap \Gamma_{\mathrm{I}} = \varnothing = \Gamma_{aD} \cap \Gamma_{\mathrm{I}}$. We further denote by $\mathbf{n}_e$ and $\mathbf{n}_a$ the outer unit normal vectors to $\partial\Omega_e$ and $\partial\Omega_a$, respectively; thereby, $\mathbf{n}_e = -\mathbf{n}_a$ on Γ_{I}. For $X \subseteq \overline{\Omega}$ or $X = \mathbb{R}^d$, we write $\mathbf{L}^2(X)$ in place of $L^2(X)^d$, with scalar product denoted by $(\cdot,\cdot)_X$ and associated norm $\|\cdot\|_X$. Analogously, we write $\mathbf{H}^l(X)$ in place of $H^l(X)^d$ for Hilbertian Sobolev spaces of vector-valued functions with index $l \geqslant 0$, equipped with norm $\|\cdot\|_{l,X}$ (so that $\|\cdot\|_{0,X} \equiv \|\cdot\|_X$ on $\mathbf{H}^0(X) \equiv \mathbf{L}^2(X)$). Given an integer $p \geqslant 1$, $\mathscr{P}_p(X)$ denotes the space spanned by polynomials of total degree at most p on X. Given a subdivision $\mathcal{T}_h$ of Ω into disjoint open elements κ such that $\overline{\Omega} = \bigcup_{\kappa\in\mathcal{T}_h} \overline{\kappa}$, we denote by

$$\mathscr{P}_{\mathbf{p}}(\mathcal{T}_h) = \{v \in L^2(\Omega) : v_{|\kappa} \in \mathscr{P}_{p_\kappa}(\kappa)\ \forall \kappa \in \mathcal{T}_h\}$$

the space of piecewise polynomial functions on $\mathcal{T}_h$, with $\mathbf{p} = (p_\kappa)_{\kappa\in\mathcal{T}_h}$, $p_\kappa \geqslant 1\ \forall \kappa \in \mathcal{T}_h$; and by . Finally, for $T > 0$, we let $(0, T]$ denote a time interval. For the sake of readibility we omit, at times, the dependence on time $t \in (0, T]$. The first and second time derivatives of a scalar- or vector-valued function $\Psi = \Psi(t)$ are denoted by $\dot{\Psi}$ and $\ddot{\Psi}$, respectively.

3. The elasto-acoustic problem

The elasto-acoustic problem is formulated as follows: given a body force $\mathbf{f}_e \colon \Omega_e \times (0, T] \to \mathbb{R}^3$, an acoustic volume source $f_a \colon \Omega_a \times (0, T] \to \mathbb{R}$, and initial conditions $\mathbf{u}_0, \mathbf{u}_1 \colon \Omega_e \to \mathbb{R}^3$ and $\varphi_0, \varphi_1 \colon \Omega_a \to \mathbb{R}$, find $\mathbf{u} \colon \Omega_e \times (0, T] \to \mathbb{R}^3$ and $\varphi \colon \Omega_a \times (0, T] \to \mathbb{R}$ such that

$$
\begin{cases}
\rho_e \ddot{\mathbf{u}} + 2\rho_e \zeta \dot{\mathbf{u}} + \rho_e \zeta^2 \mathbf{u} - \mathbf{div}\, \boldsymbol{\sigma}(\mathbf{u}) = \mathbf{f}_e & \text{in } \Omega_e \times (0, T], \\
\mathbf{u} = \mathbf{0} & \text{on } \Gamma_{eD} \times (0, T], \\
\boldsymbol{\sigma}(\mathbf{u})\mathbf{n}_e = -\rho_a \dot{\varphi}\, \mathbf{n}_e & \text{on } \Gamma_{\mathrm{I}} \times (0, T], \\
\mathbf{u}(\cdot, 0) = \mathbf{u}_0, & \text{in } \Omega_e, \\
\dot{\mathbf{u}}(\cdot, 0) = \mathbf{u}_1 & \text{in } \Omega_e; \\
c^{-2} \ddot{\varphi} - \triangle \varphi = f_a & \text{in } \Omega_a \times (0, T], \\
\varphi = 0 & \text{on } \Gamma_{aD} \times (0, T], \\
\partial \varphi / \partial \mathbf{n}_a = -\dot{\mathbf{u}} \cdot \mathbf{n}_a & \text{on } \Gamma_{\mathrm{I}} \times (0, T]; \\
\varphi(\cdot, 0) = \varphi_0, & \text{in } \Omega_a, \\
\dot{\varphi}(\cdot, 0) = \varphi_1 & \text{in } \Omega_a.
\end{cases}
\tag{1}
$$

Here, the unknowns $\mathbf{u}$ and φ represent the displacement vector and the acoustic potential, respectively. Moreover, $\boldsymbol{\sigma}(\mathbf{u}) = \mathbb{C}\boldsymbol{\varepsilon}(\mathbf{u})$ is the Cauchy stress tensor, with $\mathbb{C}$ the fourth-order, symmetric and uniformly elliptic elasticity tensor, i.e.

$$
\begin{gathered}
C_{ijk\ell} = C_{jik\ell} = C_{k\ell ij} = C_{ij\ell k}, \quad C_{ijk\ell} \in L^\infty(\Omega_e), \quad i, j, k, \ell \in \{1, 2, 3\}, \\
C_{ijk\ell} X_{k\ell} X_{ij} \geqslant \mathfrak{C} \sum_{i,j} |X_{ij}|^2 \ \text{ for all } X_{ij} = X_{ji} \in \mathbb{R},\ \mathfrak{C} > 0,
\end{gathered}
\tag{2}
$$

and $\boldsymbol{\varepsilon}(\mathbf{u}) = \frac{1}{2}\left(\boldsymbol{\nabla}\mathbf{u} + \boldsymbol{\nabla}\mathbf{u}^T\right)$ is the strain tensor. In the case where Ω_e is occupied by an *isotropic* medium, i.e., such that $\boldsymbol{\sigma}(\mathbf{u}) = 2\mu\, \boldsymbol{\varepsilon}(\mathbf{u}) + \lambda(\operatorname{div} \mathbf{u})\mathbf{I}$, μ and λ being the Lamé coefficients and $\mathbf{I}$ the identity tensor, we denote by $c_P = \sqrt{(\lambda + 2\mu)/\rho_e}$ and $c_S = \sqrt{\mu/\rho_e}$ the velocities of pressure and shear waves propagating in Ω_e, respectively. Moreover, we denote by ρ_e the density of the elastic body Ω_e, with $0 < \rho_e^- \leqslant \rho_e \leqslant \rho_e^+ < +\infty$ a.e. in Ω_e, by ρ_a the density of the acoustic region Ω_a, with $0 < \rho_a^- \leqslant \rho_a \leqslant \rho_a^+ < +\infty$ a.e. in Ω_a, and by $c > 0$ the speed of the acoustic wave.

The *damping factor* $\zeta \in L^\infty(\Omega_e)$, $\zeta \geqslant 0$, is a decay factor with the dimension of the inverse of time. Its role is to model viscoelastic effects without resorting to constitutive laws based on Prony series, which involve time convolutions to express the stress in terms of the strain history (see e.g. [61, 62]). The main idea is to regard the sum of ζ-dependent terms as a *viscous*

displacement-dependent volume force $\mathbf{f}_{vs} = -2\rho_e\zeta\dot{\mathbf{u}} - \rho_e\zeta^2\mathbf{u}$ acting upon a purely elastic body undergoing a displacement field $\mathbf{u}$ (see e.g. [63]). It can be shown that, considering an harmonic excitation, the solution $\mathbf{u}$ obtained by adding the viscous force can be related to the solution $\hat{\mathbf{u}}$ of the corresponding linear elastic problem by the relation $\mathbf{u} = e^{-\zeta t}\hat{\mathbf{u}}$. Hence, every frequency component of the solution to the linear elastic problem is attenuated by an exponential factor.

Notice that the coupled nature of the problem is to be ascribed to the trasmission conditions imposed on $\Gamma_{\mathrm{I}} \times (0,T]$. The first one takes account of the acoustic pressure exterted by the fluid onto the elastic body through the interface, whereas the second one expresses the continuity of the normal component of the velocity field at the interface.

3.1. Existence and uniqueness

The existence and uniqueness of a strong solution to (1) can be inferred in the framework of the Hille–Yosida theory. To this aim, suitable regularity assumptions are needed on source terms, as well as on initial and boundary data. Let us first introduce the Hilbertian Sobolev spaces

$$\begin{aligned} &\mathbf{H}^1_D(\Omega_e) = \{\mathbf{v} \in \mathbf{H}^1(\Omega_e) : \mathbf{v} = \mathbf{0} \text{ on } \Gamma_{eD}\}, && H^1_D(\Omega_a) = \{v \in H^1(\Omega_a) : v = 0 \text{ on } \Gamma_{aD}\}, \\ &\mathbf{H}^{\triangle}_{\mathbb{C}}(\Omega_e) = \{\mathbf{v} \in \mathbf{L}^2(\Omega_e) : \mathbf{div}\,\mathbb{C}\boldsymbol{\varepsilon}(\mathbf{v}) \in \mathbf{L}^2(\Omega_e)\}, && H^{\triangle}(\Omega_a) = \{v \in L^2(\Omega_a) : \triangle v \in L^2(\Omega_a)\}. \end{aligned} \tag{3}$$

For an integer $k \geqslant 0$ and a generic Hilbert space H, we also adopt the usual notation $C^k([0,T];H)$ for the space of functions k times continuously differentiable in $[0,T]$ belonging to H. The following result can now be stated; its proof is postponed to Section A.1 of Appendix A.

Theorem 3.1 (Existence and uniqueness)**.** *Assume that the initial data have the following regularity:*

$$\mathbf{u}_0 \in \mathbf{H}^{\triangle}_{\mathbb{C}}(\Omega_e) \cap \mathbf{H}^1_D(\Omega_e), \quad \mathbf{u}_1 \in \mathbf{H}^1_D(\Omega_e), \quad \varphi_0 \in H^{\triangle}(\Omega_a) \cap H^1_D(\Omega_a), \quad \varphi_1 \in H^1_D(\Omega_a) \tag{4}$$

and that the source terms are such that

$$\mathbf{f}_e \in C^1([0,T];\mathbf{L}^2(\Omega_e)), \quad f_a \in C^1([0,T];L^2(\Omega_a)). \tag{5}$$

Then, problem (1) *admits a unique strong solution* $(\mathbf{u},\varphi)$ *such that*

$$\begin{aligned} &\mathbf{u} \in C^2([0,T];\mathbf{L}^2(\Omega_e)) \cap C^1([0,T];\mathbf{H}^1_D(\Omega_e)) \cap C^0([0,T];\mathbf{H}^{\triangle}_{\mathbb{C}}(\Omega_e) \cap \mathbf{H}^1_D(\Omega_e)), \\ &\varphi \in C^2([0,T];L^2(\Omega_a)) \cap C^1([0,T];H^1_D(\Omega_a)) \cap C^0([0,T];H^{\triangle}(\Omega_a) \cap H^1_D(\Omega_a)). \end{aligned} \tag{6}$$

Remark 3.2 (Boundary conditions). We consider formulation (1) for ease of presentation, but more general boundary conditions, such as nonhomogeneous Dirichlet and Neumann conditions, can be taken into account, provided the data are sufficiently regular. In this case, suitable trace liftings of boundary data have to be introduced, by resorting to a one-parameter family of static problems (where the parameter is time). Then, it can be shown that a result analogous to (6) holds, provided boundary data have C^3-regularity in time (see, e.g., [64, Theorem 1.1]).

Remark 3.3 (Convexity). The above result holds without any convexity assumption on the subdomains Ω_e and Ω_a. However, in view of the forthcoming analysis of the semi-discrete problem

(cf. Section 5), it is convenient to assume that Ω_e and Ω_a are convex. This is necessary to ensure that the exact solution $(\mathbf{u}, \varphi)$ be (at least) H^2-regular, so that both traces of $\boldsymbol{\nabla}\mathbf{u}$ and $\boldsymbol{\nabla}\varphi$ on $(d-1)$-dimensional simplices are well defined. The present analysis can be extended to the case of non-convex domains Ω_e and Ω_a, but the semi-discrete formulation (16) has to be replaced by its not-strongly consistent version based on the lifting operators (see [12] for the purely elastic case and [65] for a diffusion equation). As a consequence, the analysis gets more involved and is based on employing Strang's lemma. For the sake of brevity, we focus here on the case of convex elastic and acoustic subdomains.

With a view towards introducing the semi-discrete counterpart of (1) and to carry out its analysis, we observe that the solution $(\mathbf{u}, \varphi)$ given by (6) satisfies the following *weak form* of (1): for any $t \in (0, T]$, and all $(\mathbf{v}, \psi) \in \mathbf{H}^1_D(\Omega_e) \times H^1_D(\Omega_a)$,

$$\begin{aligned}(\rho_e \ddot{\mathbf{u}}(t), \mathbf{v})_{\Omega_e} + (c^{-2}\rho_a \ddot{\varphi}(t), \psi)_{\Omega_a} + (2\rho_e \zeta \dot{\mathbf{u}}(t), \mathbf{v})_{\Omega_e} + (\rho_e \zeta^2 \mathbf{u}(t), \mathbf{v})_{\Omega_e} \\ + \mathcal{A}_e(\mathbf{u}(t), \mathbf{v}) + \mathcal{A}_a(\varphi(t), \psi) + \mathcal{I}_e(\dot{\varphi}(t), \mathbf{v}) + \mathcal{I}_a(\dot{\mathbf{u}}(t), \psi) \\ = (\mathbf{f}_e(t), \mathbf{v})_{\Omega_e} + (\rho_a f_a(t), \psi)_{\Omega_a}.\end{aligned} \tag{7}$$

Here, the bilinear forms $\mathcal{A}_e \colon \mathbf{H}^1_D(\Omega_e) \times \mathbf{H}^1_D(\Omega_e) \to \mathbb{R}$, $\mathcal{I}_e \colon H^{1/2}(\Gamma^a_{\mathrm{I}}) \times \mathbf{H}^{1/2}(\Gamma^e_{\mathrm{I}}) \to \mathbb{R}$, $\mathcal{A}_a \colon H^1_D(\Omega_a) \times H^1_D(\Omega_a) \to \mathbb{R}$, and $\mathcal{I}_a \colon \mathbf{H}^{1/2}(\Gamma^e_{\mathrm{I}}) \times H^{1/2}(\Gamma^a_{\mathrm{I}}) \to \mathbb{R}$ are defined as follows:

$$\begin{aligned}\mathcal{A}_e(\mathbf{u}, \mathbf{v}) &= (\mathbb{C}\boldsymbol{\varepsilon}(\mathbf{u}), \boldsymbol{\varepsilon}(\mathbf{v}))_{\Omega_e}, & \mathcal{I}_e(\psi, \mathbf{v}) &= (\rho_a \psi \mathbf{n}_e, \mathbf{v})_{\Gamma_{\mathrm{I}}}, \\ \mathcal{A}_a(\varphi, \psi) &= (\rho_a \boldsymbol{\nabla}\varphi, \boldsymbol{\nabla}\psi)_{\Omega_a}, & \mathcal{I}_a(\mathbf{v}, \psi) &= (\rho_a \mathbf{v}\cdot\mathbf{n}_a, \psi)_{\Gamma_{\mathrm{I}}},\end{aligned} \tag{8}$$

where we have used the spaces of traces $\mathbf{H}^{1/2}(\Gamma^e_{\mathrm{I}})$ and $H^{1/2}(\Gamma^a_{\mathrm{I}})$ of functions of $\mathbf{H}^1(\Omega_e) \supset \mathbf{H}^1_D(\Omega_e)$ and $H^1(\Omega_a) \supset H^1_D(\Omega_a)$ on Γ_{I}, respectively [66, 67]. Notice that we have multiplied the second evolution equation by ρ_a to ensure (skew) symmetry of the two interface terms (since $\mathbf{n}_a = -\mathbf{n}_e$).

4. Discrete setting

Assuming that Ω_e and Ω_a are polygonal or polyhedral domains, we now introduce a polytopic mesh $\mathcal{T}_h$ over Ω. We denote by h_κ the diameter of an element $\kappa \in \mathcal{T}_h$, and set $h = \max_{\kappa\in\mathcal{T}_h} h_\kappa$. We assume that $\mathcal{T}_h$ is *compliant with the underlying geometry*, i.e., the decomposition $\mathcal{T}_h = \mathcal{T}^e_h \cup \mathcal{T}^a_h$ holds, where $\mathcal{T}^e_h = \{\kappa \in \mathcal{T}_h : \overline{\kappa} \subseteq \overline{\Omega}_e\}$ and $\mathcal{T}^a_h = \{\kappa \in \mathcal{T}_h : \overline{\kappa} \subseteq \overline{\Omega}_a\}$. We assume that $\mathbb{C}$ and ρ_a are element-wise constant, and set

$$\overline{\mathbb{C}}_\kappa = (|\mathbb{C}^{1/2}|^2_2)_{|\kappa} \quad \forall \kappa \in \mathcal{T}^e_h, \qquad \overline{\rho}_{a,\kappa} = \rho_{a|\kappa} \quad \forall \kappa \in \mathcal{T}^a_h. \tag{9}$$

Here we have denoted by $|\cdot|_2$ the operator norm induced by the ℓ^2-norm on $\mathbb{R}^n$, with n the dimension of the space of symmetric second-order tensors ($n = 3$ if $d = 2$, $n = 6$ if $d = 3$). With each element of $\mathcal{T}^e_h$ (resp. $\mathcal{T}^a_h$), we associate a polynomial degree $p_{e,\kappa} \geqslant 1$ (resp. $p_{a,\kappa} \geqslant 1$), and introduce the following finite-dimensional spaces:

$$\begin{aligned}\mathbf{V}^e_h &= [\mathscr{P}_{\mathbf{p}_e}(\mathcal{T}^e_h)]^d = \left\{\mathbf{v}_h \in \mathbf{L}^2(\Omega_e) : \mathbf{v}_{h|\kappa} \in [\mathscr{P}_{p_{e,\kappa}}(\kappa)]^d \ \forall \kappa \in \mathcal{T}^e_h\right\}, \\ V^a_h &= \mathscr{P}_{\mathbf{p}_a}(\mathcal{T}^a_h) = \left\{\psi_h \in L^2(\Omega_a) : \psi_{h|\kappa} \in \mathscr{P}_{p_{a,\kappa}}(\kappa) \ \forall \kappa \in \mathcal{T}^a_h\right\}.\end{aligned}$$

For an integer $l \geqslant 1$, we also introduce the broken Sobolev spaces

$$\begin{aligned} \mathbf{H}^l(\mathcal{T}_h^e) &= \left\{ \mathbf{v} \in \mathbf{L}^2(\Omega_e) \,:\, \mathbf{v}_{|\kappa} \in \mathbf{H}^l(\kappa) \;\forall \kappa \in \mathcal{T}_h^e \right\}, \\ H^l(\mathcal{T}_h^a) &= \left\{ \psi \in L^2(\Omega_a) \,:\, \psi_{|\kappa} \in H^l(\kappa) \;\forall \kappa \in \mathcal{T}_h^a \right\}. \end{aligned} \tag{10}$$

Henceforth, we write $x \lesssim y$ and $x \gtrsim y$ in place of $x \leqslant Cy$ and $x \geqslant Cy$ respectively, for $C > 0$ independent of the discretization parameters (polynomial degree and meshsize), as well as of the number of faces of a mesh element, but possibly depending on material properties, such as $\mathbb{C}$, ρ_e, c, and ρ_a.

4.1. Grid assumptions

We term *interface* of $\mathcal{T}_h$ the intersection of the boundaries of any two neighboring elements of $\mathcal{T}_h$. This definition allows for the treatment of situations where hanging nodes or edges are present. Therefore, for $d = 2$, an interface will always consist of a piecewise linear segment. On the other hand, for $d = 3$, an interface will be given by the union of general polygonal surfaces; we thereby assume that each planar section of a given interface may be subdivided into a set of co-planar triangles. We refer to such $(d-1)$-dimensional simplices (line segments for $d = 2$, triangles for $d = 3$), whose union determines an interface of $\mathcal{T}_h$, as *faces*. We denote by $\mathcal{F}_h$ the set of all faces of $\mathcal{T}_h$. Also, let

$$\mathcal{T}_{h,\mathrm{I}} = \{\kappa \in \mathcal{T}_h : \partial\kappa \cap \Gamma_{\mathrm{I}} \neq \varnothing\} \tag{11}$$

denote the set of elements sharing a part of their boundary with Γ_{I}, and $\mathcal{T}_{h,\mathrm{I}}^e = \mathcal{T}_{h,\mathrm{I}} \cap \mathcal{T}_h^e$, $\mathcal{T}_{h,\mathrm{I}}^a = \mathcal{T}_{h,\mathrm{I}} \cap \mathcal{T}_h^a$. We then define the set of faces laying on Γ_{I} as follows:

$$\mathcal{F}_{h,\mathrm{I}} = \{F \in \mathcal{F}_h : F \subset \partial\kappa^e \cap \partial\kappa^a,\ \kappa^e \in \mathcal{T}_{h,\mathrm{I}}^e,\ \kappa^a \in \mathcal{T}_{h,\mathrm{I}}^a\} \tag{12}$$

(see Figure 2). Hence, we assume the following decomposition: $\mathcal{F}_h = \mathcal{F}_h^e \cup \mathcal{F}_{h,\mathrm{I}} \cup \mathcal{F}_h^a$, where $\mathcal{F}_h^e$ and $\mathcal{F}_h^a$ collect, respectively, all faces of $\mathcal{T}_h^e$ and of $\mathcal{T}_h^a$ that *do not lay* on Γ_{I}. Further, $\mathcal{F}_h^e$ and $\mathcal{F}_h^a$ are decomposed as follows: $\mathcal{F}_h^e = \mathcal{F}_h^{e,\mathrm{i}} \cup \mathcal{F}_h^{e,\mathrm{b}}$, $\mathcal{F}_h^a = \mathcal{F}_h^{a,\mathrm{i}} \cup \mathcal{F}_h^{a,\mathrm{b}}$, where $\mathcal{F}_h^{e,\mathrm{i}}$ and $\mathcal{F}_h^{a,\mathrm{i}}$ collect the *internal faces* of $\mathcal{T}_h^e$ and $\mathcal{T}_h^a$, respectively, and $\mathcal{F}_h^{e,\mathrm{b}}$, $\mathcal{F}_h^{a,\mathrm{b}}$ collect the *boundary faces* of $\mathcal{T}_h^e$ and $\mathcal{T}_h^a$, respectively.

We can now proceed to state the main assumptions on $\mathcal{T}_h$, referring to [19, Chapter 4] and to [14, 15] for further details.

Assumption 1a (Generalized shape-regularity)**.** For any element $\kappa \in \mathcal{T}_h$, there exists a set of non-overlapping (not necessarily shape-regular) d-dimensional simplices $\{\kappa_\flat^F\}_{F\subset\partial\kappa} \subset \kappa$, each one of them sharing the specific face $F \subset \partial\kappa$ with κ, such that, for any face $F \subset \partial\kappa$,

$$\text{(i) } h_\kappa \lesssim \frac{d|\kappa_\flat^F|}{|F|}, \qquad \text{(ii) } \bigcup_{F\subset\partial\kappa} \overline{\kappa}_\flat^F \subseteq \overline{\kappa}, \tag{13}$$

where the hidden constant is independent of the discretization parameters, the number of faces of κ, the measure of F, and the material properties.

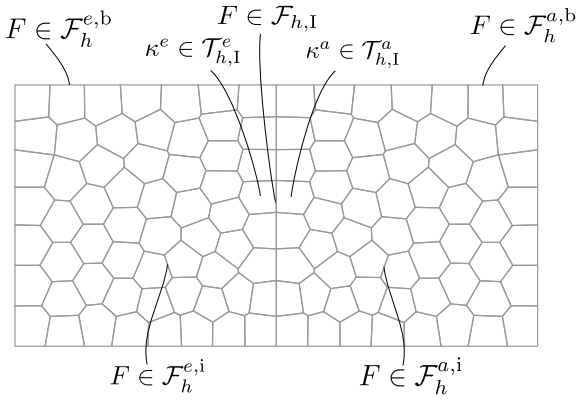

Figure 2: Explanation of the employed notation for mesh elements and faces, in a two-dimensional setting. The left domain is elastic, the right one acoustic.

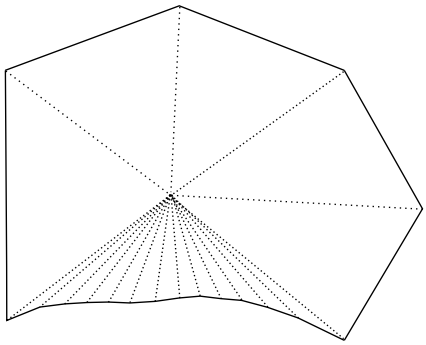

Figure 3: A possible element of $\mathcal{T}_h$ satisfying Assumption 1a with many tiny faces.

Remark 4.1 (Number of faces and degenerating faces). Notice that no restriction is imposed by Assumption 1a on either the number of faces of an element, or the measure of the face of an element with respect to the diameter of the element itself (cf. Figure 3). Therefore, the case of faces degenerating under mesh refinement can be considered as well. The first condition in (13) requires that, for a given face F, the diameter of a given mesh element is comparable with the height of any d-simplex $\kappa_\flat^F$ having F as a base.

We recall that, under Assumption 1a, the following *trace-inverse inequality* holds for polytopic elements:

$$\forall \kappa \in \mathcal{T}_h,\ \forall v \in \mathscr{P}_p(\kappa), \quad \|v\|_{\partial\kappa} \lesssim p h_\kappa^{-1/2} \|v\|_\kappa, \tag{14}$$

where the hidden constant is independent of the discretization parameters, the number of faces per element, and the material properties [14, 15, 19].

Assumption 1b (Covering simplicial mesh)**.** Let $\mathcal{T}_h^\sharp = \{\mathcal{K}\}$ denote a *covering* of $\Omega = \Omega_e \cup \Omega_a$, given by the union of two disjoint coverings $\mathcal{T}_h^{\sharp,e}$ and $\mathcal{T}_h^{\sharp,a}$, consisting of shape-regular d-dimensional simplices $\mathcal{K}$ (cf. Figure 4). We assume that, for any $\kappa \in \mathcal{T}_h$, there exists $\mathcal{K} \in \mathcal{T}_h^\sharp$

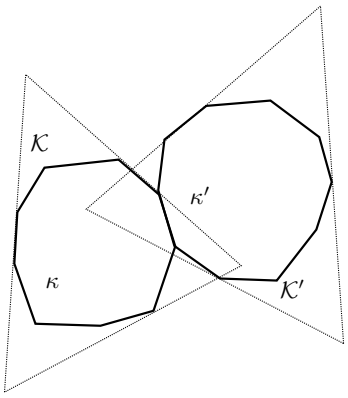

Figure 4: Two elements of $\mathcal{T}_h$ and the corresponding elements of $\mathcal{T}_h^\sharp$.

such that $\kappa \subset \mathcal{K}$ and

$$\max_{\kappa \in \mathcal{T}_h} \operatorname{card} \left\{ \kappa' \in \mathcal{T}_h : \kappa' \cap \mathcal{K} \neq \varnothing,\ \mathcal{K} \in \mathcal{T}_h^\sharp \text{ such that } \kappa \subset \mathcal{K} \right\} \lesssim 1; \tag{15}$$

and that, for each pair $\kappa \in \mathcal{T}_h$, $\mathcal{K} \in \mathcal{T}_h^\sharp$ with $\kappa \subset \mathcal{K}$, $\operatorname{diam}(\mathcal{K}) \lesssim h_\kappa$, where the hidden constant is independent of the discretization parameters and of the material properties. Inequality (15) sets a bound on the maximum amount of overlap between elements in $\mathcal{T}_h$ and the simplices of the covering mesh $\mathcal{T}_h^\sharp$; we refer the reader to [19, Section 3.3] for further details.

Assumption 1c (hp-local quasi-uniformity)**.** Given any two neighboring elements κ^-, $\kappa^+ \in \mathcal{T}_h$, it holds

$$h_{\kappa^+} \lesssim h_{\kappa^-} \lesssim h_{\kappa^+}, \quad p_{\kappa^+} \lesssim p_{\kappa^-} \lesssim p_{\kappa^+},$$

where the hidden constants, lower and greater than one in the left and right sides, respectively, are independent of the discretization parameters, the number of faces per element, and the material properties. For details, see e.g. [65, 68] as well as the very recent contribution by Lozinski [69].

5. Semi-discrete problem

In this section, as well as in the following, we suppose that the solution to (1) is such that $\mathbf{u} \in C^2([0,T]; \mathbf{H}^2(\Omega_e) \cap \mathbf{H}^m(\mathcal{T}_h^e))$ and $\varphi \in C^2([0,T]; H^2(\Omega_a) \cap H^n(\mathcal{T}_h^a))$, with $m, n > 2$ (cf. Remark 3.3). Before stating the dG formulation of the semi-discrete problem we introduce the following average and jump operators [1, 70]. For sufficiently smooth scalar-, vector- and tensor-valued fields ψ, $\mathbf{v}$, and τ, we define averages and jumps on an internal face $F \in \mathcal{F}_h^{e,\mathrm{i}} \cup \mathcal{F}_h^{a,\mathrm{i}}$, $F \subset \partial\kappa^+ \cap \partial\kappa^-$ with κ^+ and κ^- any two neighboring elements in $\mathcal{T}_h^e$ or $\mathcal{T}_h^a$, as follows:

$$\begin{aligned}
&[\![\psi]\!] = \psi^+ \mathbf{n}^+ + \psi^- \mathbf{n}^-, && \{\!\{\psi\}\!\} = \frac{\psi^+ + \psi^-}{2}, \\
&[\![\mathbf{v}]\!] = \mathbf{v}^+ \otimes \mathbf{n}^+ + \mathbf{v}^- \otimes \mathbf{n}^-, && \{\!\{\mathbf{v}\}\!\} = \frac{\mathbf{v}^+ + \mathbf{v}^-}{2}, \\
&[\![\tau]\!] = \tau^+ \mathbf{n}^+ + \tau^- \mathbf{n}^-, && \{\!\{\tau\}\!\} = \frac{\tau^+ + \tau^-}{2},
\end{aligned}$$

where $\mathbf{a}\otimes\mathbf{b}$ denotes the tensor product of $\mathbf{a},\mathbf{b}\in\mathbb{R}^3$, and $\psi^\pm$, $\mathbf{v}^\pm$ and $\tau^\pm$ denote the zeroth-order traces of ψ, $\mathbf{v}$ and τ on F taken from the interior of $\kappa^\pm$, and $\mathbf{n}^\pm$ is the outer unit normal vector to $\partial\kappa^\pm$. When considering a boundary face $F\in\mathcal{F}_h^{e,\mathrm{b}}\cup\mathcal{F}_h^{a,\mathrm{b}}$, we set $[\![\psi]\!]=\psi\mathbf{n}$, $[\![\mathbf{v}]\!]=\mathbf{v}\otimes\mathbf{n}$, $[\![\tau]\!]=\tau\mathbf{n}$, and $\{\!\{\psi\}\!\}=\psi$, $\{\!\{\mathbf{v}\}\!\}=\mathbf{v}$, $\{\!\{\tau\}\!\}=\tau$. We also use the shorthand notation

$$\langle\Phi,\Psi\rangle_{\mathcal{F}}=\sum_{F\in\mathcal{F}}(\Phi,\Psi)_F,\qquad\|\Phi\|_{\mathcal{F}}=\langle\Phi,\Phi\rangle_{\mathcal{F}}^{1/2}$$

for scalar, vector or tensor fields Φ and Ψ and for a generic collection of faces $\mathcal{F}\subset\mathcal{F}_h$.

The semi-discrete approximation of problem (7) reads: find $(\mathbf{u}_h,\varphi_h)\in C^2([0,T];\mathbf{V}_h^e)\times C^2([0,T];V_h^a)$ such that, for all $(\mathbf{v}_h,\psi_h)\in\mathbf{V}_h^e\times V_h^a$,

$$\begin{aligned}&(\rho_e\ddot{\mathbf{u}}_h(t),\mathbf{v}_h)_{\Omega_e}+(c^{-2}\rho_a\ddot{\varphi}_h(t),\psi_h)_{\Omega_a}+(2\rho\zeta\dot{\mathbf{u}}_h(t),\mathbf{v}_h)_{\Omega_e}+(\rho\zeta^2\mathbf{u}_h(t),\mathbf{v}_h)_{\Omega_e}\\&\quad+\mathcal{A}_h^e(\mathbf{u}_h(t),\mathbf{v}_h)+\mathcal{A}_h^a(\varphi_h(t),\psi_h)+\mathcal{I}_h^e(\dot{\varphi}_h(t),\mathbf{v}_h)+\mathcal{I}_h^a(\dot{\mathbf{u}}_h(t),\psi_h)\\&\qquad=(\mathbf{f}_e(t),\mathbf{v}_h)_{\Omega_e}+(\rho_a f_a(t),\psi_h)_{\Omega_a},\end{aligned}\tag{16}$$

with initial conditions $(\mathbf{u}_h(0),\dot{\mathbf{u}}_h(0),\varphi_h(0),\dot{\varphi}_h(0))\in\mathbf{V}_h^e\times\mathbf{V}_h^e\times V_h^a\times V_h^a$, where the bilinear forms $\mathcal{A}_h\colon\mathbf{V}_h^e\times\mathbf{V}_h^e\to\mathbb{R}$, $\mathcal{A}_h^a\colon V_h^a\times V_h^a\to\mathbb{R}$, $\mathcal{I}_h^e\colon V_h^a\times\mathbf{V}_h^e\to\mathbb{R}$ and $\mathcal{I}_h^a\colon\mathbf{V}_h^e\times V_h^a\to\mathbb{R}$ are given by

$$\begin{aligned}\mathcal{A}_h^e(\mathbf{u},\mathbf{v})&=(\boldsymbol{\sigma}_h(\mathbf{u}),\boldsymbol{\varepsilon}_h(\mathbf{v}))_{\Omega_e}-\langle\{\!\{\boldsymbol{\sigma}_h(\mathbf{u})\}\!\},[\![\mathbf{v}]\!]\rangle_{\mathcal{F}_h^e}-\langle[\![\mathbf{u}]\!],\{\!\{\boldsymbol{\sigma}_h(\mathbf{v})\}\!\}\rangle_{\mathcal{F}_h^e}+\langle\eta[\![\mathbf{u}]\!],[\![\mathbf{v}]\!]\rangle_{\mathcal{F}_h^e}\\\mathcal{A}_h^a(\varphi,\psi)&=(\rho_a\boldsymbol{\nabla}_h\varphi,\boldsymbol{\nabla}_h\psi)_{\Omega_a}-\langle\{\!\{\rho_a\boldsymbol{\nabla}_h\varphi\}\!\},[\![\psi]\!]\rangle_{\mathcal{F}_h^a}-\langle[\![\varphi]\!],\{\!\{\rho_a\boldsymbol{\nabla}_h\psi\}\!\}\rangle_{\mathcal{F}_h^a}+\langle\chi[\![\varphi]\!],[\![\psi]\!]\rangle_{\mathcal{F}_h^a}\\\mathcal{I}_h^e(\psi,\mathbf{v})&=(\rho_a\psi\mathbf{n}_e,\mathbf{v})_{\Gamma_\mathrm{I}},\quad\mathcal{I}_h^a(\mathbf{v},\psi)=(\rho_a\mathbf{v}\cdot\mathbf{n}_a,\psi)_{\Gamma_\mathrm{I}}=-\mathcal{I}_h^e(\psi,\mathbf{v}),\end{aligned}\tag{17}$$

with $\boldsymbol{\nabla}_h$ the usual broken gradient operator on $\mathcal{T}_h$. We point out that the last identity in (17) holds due to the fact that $\mathbf{n}_a=-\mathbf{n}_e$. Here we have set, for any integer $l\geqslant 1$ and any $\mathbf{v}\in\mathbf{H}^l(\mathcal{T}_h^e)\supset\mathbf{V}_h^e$,

$$\boldsymbol{\varepsilon}_h(\mathbf{v})=\frac{1}{2}\left(\boldsymbol{\nabla}_h\mathbf{v}+\boldsymbol{\nabla}_h\mathbf{v}^T\right),\quad\boldsymbol{\sigma}_h(\mathbf{v})=\mathbb{C}\boldsymbol{\varepsilon}_h(\mathbf{v}).$$

The *stabilization functions* $\eta\in L^\infty(\mathcal{F}_h^e)$ and $\chi\in L^\infty(\mathcal{F}_h^a)$ are defined as follows:

$$\eta_{|F}=\begin{cases}\alpha\max\limits_{\kappa\in\{\kappa^+,\kappa^-\}}\left(\dfrac{\overline{\mathbb{C}}_\kappa p_{e,\kappa}^2}{h_\kappa}\right)&\forall F\in\mathcal{F}_h^{e,\mathrm{i}},\quad F\subseteq\partial\kappa^+\cap\partial\kappa^-,\\\dfrac{\overline{\mathbb{C}}_\kappa p_{e,\kappa}^2}{h_\kappa}&\forall F\in\mathcal{F}_h^{e,\mathrm{b}},\quad F\subseteq\partial\kappa;\end{cases}\tag{18a}$$

$$\chi_{|F}=\begin{cases}\beta\max\limits_{\kappa\in\{\kappa^+,\kappa^-\}}\left(\dfrac{\overline{\rho}_{a,\kappa}p_{a,\kappa}^2}{h_\kappa}\right)&\forall F\in\mathcal{F}_h^{a,\mathrm{i}},\quad F\subseteq\partial\kappa^+\cap\partial\kappa^-,\\\dfrac{\overline{\rho}_{a,\kappa}p_{a,\kappa}^2}{h_\kappa}&\forall F\in\mathcal{F}_h^{a,\mathrm{b}},\quad F\subseteq\partial\kappa,\end{cases}\tag{18b}$$

cf. in particular [19, Lemma 35] for second-order elliptic problems. In (18a)-(18b), $\alpha,\beta>0$ are

constants to be properly chosen. We now introduce the following norms:

$$\begin{aligned}
\|\mathbf{v}\|^2_{\mathrm{dG},e} &= \|\mathbb{C}^{1/2}\boldsymbol{\varepsilon}_h(\mathbf{v})\|^2_{\Omega_e} + \|\eta^{1/2}[\![\mathbf{v}]\!]\|^2_{\mathcal{F}_h^e} \qquad \forall \mathbf{v} \in \mathbf{H}^1(\mathcal{T}_h^e) \supset \mathbf{V}_h^e,\\
|||\mathbf{v}|||^2_{\mathrm{dG},e} &= \|\mathbf{v}\|^2_{\mathrm{dG},e} + \|\eta^{-1/2}\{\!\{\mathbb{C}\boldsymbol{\varepsilon}_h(\mathbf{v})\}\!\}\|^2_{\mathcal{F}_h^e} \qquad \forall \mathbf{v} \in \mathbf{H}^2(\mathcal{T}_h^e),\\
\|\psi\|^2_{\mathrm{dG},a} &= \|\rho_a^{1/2}\boldsymbol{\nabla}_h\psi\|^2_{\Omega_a} + \|\chi^{1/2}[\![\psi]\!]\|^2_{\mathcal{F}_h^a} \qquad \forall \psi \in H^1(\mathcal{T}_h^a) \supset V_h^a,\\
|||\psi|||^2_{\mathrm{dG},a} &= \|\psi\|^2_{\mathrm{dG},a} + \|\chi^{-1/2}\{\!\{\rho_a\boldsymbol{\nabla}_h\psi\}\!\}\|^2_{\mathcal{F}_h^a} \qquad \forall \psi \in H^2(\mathcal{T}_h^a).
\end{aligned} \tag{19}$$

The following result follows based on employing standard arguments.

Lemma 5.1 (Coercivity and boundedness of $\mathcal{A}_h^e$ and $\mathcal{A}_h^a$)**.** *Provided that $\mathcal{T}_h$ satisfies Assumption 1a, and that constants α and β are chosen sufficiently large, the following continuity and coercivity bounds hold:*

$$\begin{aligned}
\mathcal{A}_h^e(\mathbf{u},\mathbf{v}) &\lesssim \|\mathbf{u}\|_{\mathrm{dG},e}\|\mathbf{v}\|_{\mathrm{dG},e} \qquad \forall \mathbf{u},\mathbf{v} \in \mathbf{V}_h^e,\\
\mathcal{A}_h^e(\mathbf{v},\mathbf{v}) &\gtrsim \|\mathbf{v}\|^2_{\mathrm{dG},e} \qquad \forall \mathbf{v} \in \mathbf{V}_h^e,
\end{aligned} \tag{20a}$$

$$\begin{aligned}
\mathcal{A}_h^a(\varphi,\psi) &\lesssim \|\varphi\|_{\mathrm{dG},a}\|\psi\|_{\mathrm{dG},a} \qquad \forall \varphi,\psi \in V_h^a,\\
\mathcal{A}_h^a(\psi,\psi) &\gtrsim \|\psi\|^2_{\mathrm{dG},a} \qquad \forall \psi \in V_h^a.
\end{aligned} \tag{20b}$$

Moreover,

$$\begin{aligned}
\mathcal{A}_h^e(\mathbf{w},\mathbf{v}) &\lesssim |||\mathbf{w}|||_{\mathrm{dG},e}\|\mathbf{v}\|_{\mathrm{dG},e} \qquad \forall \mathbf{w},\mathbf{v} \in \mathbf{H}^2(\mathcal{T}_h^e) + \mathbf{V}_h^e,\\
\mathcal{A}_h^a(\varphi,\psi) &\lesssim |||\varphi|||_{\mathrm{dG},a}\|\psi\|_{\mathrm{dG},a} \qquad \forall \varphi,\psi \in H^2(\mathcal{T}_h^a) + V_h^a.
\end{aligned} \tag{21}$$

The proof of the above result is based on arguments along the same lines as in the proof of Lemma A.II in the Appendix. As a consequence of (20a)–(20b), whose proof hinges on Lemma A.I, the theory of ordinary differential equations guarantees that problem (16) admits a unique solution (notice, also, that the coupling terms stemming from bilinear forms $\mathcal{I}_h^e$ and $\mathcal{I}_h^a$ do not contribute to the energy of the system, cf. Remark 6.1 below).

6. Stability of the semi-discrete formulation

In this section we state a stability result for the semi-discrete problem (16), i.e., the continuous dependency of the semi-discrete solution on the data (see [71, 72, 68, 12] for the purely elastic case). The proof is postponed to Section A.2 of Appendix A. Let $\mathbf{W} = (\mathbf{v},\psi) \in C^1([0,T];\mathbf{V}_h^e) \times C^1([0,T];V_h^a)$; we introduce the following mesh-dependent *energy norm*:

$$\|\mathbf{W}(t)\|^2_{\mathcal{E}} = \|\mathbf{v}(t)\|^2_{\mathcal{E}_e} + \|\psi(t)\|^2_{\mathcal{E}_a}, \tag{22}$$

where

$$\begin{aligned}
\|\mathbf{v}(t)\|^2_{\mathcal{E}_e} &= \|\rho_e^{1/2}\dot{\mathbf{v}}(t)\|^2_{\Omega_e} + \|\rho_e^{1/2}\zeta\mathbf{v}(t)\|^2_{\Omega_e} + \|\mathbf{v}(t)\|^2_{\mathrm{dG},e},\\
\|\psi(t)\|^2_{\mathcal{E}_a} &= \|c^{-1}\rho_a^{1/2}\dot{\psi}(t)\|^2_{\Omega_a} + \|\psi(t)\|^2_{\mathrm{dG},a}.
\end{aligned} \tag{23}$$

Remark 6.1 (Energy norm). The definition of the energy norm does not take into account the interface terms. The reason is related to the fact that, as observed previously, the bilinear forms $\mathcal{I}_h^e$ and $\mathcal{I}_h^a$ are skew-symmetric, i.e., $\mathcal{I}_h^a(\mathbf{v},\psi) = -\mathcal{I}_h^e(\psi,\mathbf{v})$ for all $(\mathbf{v},\psi) \in \mathbf{V}_h^e \times V_h^a$.

Theorem 6.2 (Stability of the semi-discrete formulation)**.** *For any $t \in (0,T]$, let $\mathbf{U}_h = (\mathbf{u}_h, \varphi_h)$ be the solution of (16). Let Assumptions 1a and 1c be satisfied. For sufficiently large penalty parameters α and β in (18a) and (18b), respectively, the following bound holds:*

$$\|\mathbf{U}_h(t)\|_{\mathcal{E}} \lesssim \|\mathbf{U}_h(0)\|_{\mathcal{E}} + \int_0^t \left(\|\mathbf{f}_e(\tau)\|_{\Omega_e} + \|f_a(\tau)\|_{\Omega_a}\right) \mathrm{d}\tau, \quad t \in (0,T]. \tag{24}$$

7. Semi-discrete error estimate

In this section we state an *a priori* error estimate for the semi-discrete coupled problem (16). For an open bounded polytopic domain $D \subset \mathbb{R}^d$, and a generic polytopic mesh $\mathcal{T}_h$ over D satisfying Assumption 1b, we introduce, for any $\kappa \in \mathcal{T}_h$ and $m \in \mathbb{N}_0$, the *extension operator* $\mathscr{E}\colon H^m(\kappa) \to H^m(\mathbb{R}^d)$ such that $\mathscr{E}v_{|\kappa} = v$, $\|\mathscr{E}v\|_{m,\mathbb{R}^d} \lesssim \|v\|_{m,\kappa}$. The corresponding vector-valued version, mapping $\mathbf{H}^m(\kappa)$ onto $\mathbf{H}^m(\mathbb{R}^d)$, acts component-wise and is denoted in the same way. The result below is a consequence of the *hp*-approximation properties stated in [19, Lemmas 23 and 33] and of Assumption 1b.

Lemma 7.1 (Interpolation estimates)**.** *For any pair of functions $(\mathbf{v}, \psi) \in \mathbf{H}^m(\mathcal{T}_h^e) \times H^n(\mathcal{T}_h^a)$, $m \geqslant 2$, $n \geqslant 2$, there exists $(\mathbf{v}_I, \psi_I) \in \mathbf{V}_h^e \times V_h^a$ such that*

$$|||\mathbf{v} - \mathbf{v}_I|||_{\mathrm{dG},e}^2 \lesssim \sum_{\kappa \in \mathcal{T}_h^e} \frac{h_\kappa^{2\min(m,p_{e,\kappa}+1)-2}}{p_{e,\kappa}^{2m-3}} \|\mathscr{E}\mathbf{v}\|_{m,\mathcal{K}}^2,$$

$$|||\psi - \psi_I|||_{\mathrm{dG},a}^2 \lesssim \sum_{\kappa \in \mathcal{T}_h^a} \frac{h_\kappa^{2\min(n,p_{a,\kappa}+1)-2}}{p_{a,\kappa}^{2n-3}} \|\mathscr{E}\psi\|_{n,\mathcal{K}}^2.$$

Additionally, if $(\mathbf{v}, \psi) \in C^1([0,T]; \mathbf{H}^m(\mathcal{T}_h^e)) \times C^1([0,T]; H^n(\mathcal{T}_h^a))$, $m \geqslant 2$, $n \geqslant 2$, then

$$\|\mathbf{v} - \mathbf{v}_I\|_{\mathcal{E}_e}^2 \lesssim \sum_{\kappa \in \mathcal{T}_h^e} \frac{h_\kappa^{2\min(m,p_{e,\kappa}+1)-2}}{p_{e,\kappa}^{2m-3}} \left(\|\mathscr{E}\dot{\mathbf{v}}\|_{m,\mathcal{K}}^2 + \|\mathscr{E}\mathbf{v}\|_{m,\mathcal{K}}^2\right),$$

$$\|\psi - \psi_I\|_{\mathcal{E}_a}^2 \lesssim \sum_{\kappa \in \mathcal{T}_h^a} \frac{h_\kappa^{2\min(n,p_{a,\kappa}+1)-2}}{p_{a,\kappa}^{2n-3}} \left(\|\mathscr{E}\dot{\psi}\|_{n,\mathcal{K}}^2 + \|\mathscr{E}\psi\|_{n,\mathcal{K}}^2\right).$$

The proof of the following result is postponed to Section A.3 of Appendix A.

Theorem 7.1 (*A priori* error estimate in the energy norm)**.** *Let Assumptions 1a–1c hold. Assume that the exact solution of problem (1) is such that $\mathbf{u} \in C^2([0,T]; \mathbf{H}^2(\Omega_e) \cap \mathbf{H}^m(\mathcal{T}_h^e))$ and $\varphi \in C^2([0,T]; H^2(\Omega_a) \cap H^n(\mathcal{T}_h^a))$, with $m, n \geqslant 2$. Let $(\mathbf{u}_h, \varphi_h) \in C^2([0,T]; \mathbf{V}_h^e) \times C^2([0,T]; V_h^a)$ be the corresponding solution of the semi-discrete problem (16), with sufficiently large penalty parameters α and β in (18a)–(18b). Then, the following bound holds for the discretization error $\mathbf{E}(t) = (\mathbf{e}_e(t), e_a(t)) = (\mathbf{u}(t) - \mathbf{u}_h(t), \varphi(t) - \varphi_h(t))$:*

$$\sup_{t\in[0,T]} \|\mathbf{E}(t)\|_{\mathcal{E}}^2 \lesssim \sup_{t\in[0,T]} \left(\sum_{\kappa \in \mathcal{T}_h^e} \frac{h_\kappa^{2\min(m,p_{e,\kappa}+1)-2}}{p_{e,\kappa}^{2m-3}} \left(\|\mathscr{E}\dot{\mathbf{u}}\|_{m,\mathcal{K}}^2 + \|\mathscr{E}\mathbf{u}\|_{m,\mathcal{K}}^2\right) \right.$$

$$+\sum_{\kappa\in\mathcal{T}_h^a}\frac{h_\kappa^{2\min(n,p_{a,\kappa}+1)-2}}{p_{a,\kappa}^{2n-3}}\left(\|\mathscr{E}\dot{\varphi}\|_{n,\mathcal{K}}^2+\|\mathscr{E}\varphi\|_{n,\mathcal{K}}^2\right)\Bigg) \tag{25}$$

$$+\int_0^T\Bigg(\sum_{\kappa\in\mathcal{T}_h^e}\frac{h_\kappa^{2\min(m,p_{e,\kappa}+1)-2}}{p_{e,\kappa}^{2m-3}}\left(\|\mathscr{E}\ddot{\mathbf{u}}\|_{m,\mathcal{K}}^2+\|\mathscr{E}\dot{\mathbf{u}}\|_{m,\mathcal{K}}^2+\|\mathscr{E}\mathbf{u}\|_{m,\mathcal{K}}^2\right)$$

$$+\sum_{\kappa\in\mathcal{T}_h^a}\frac{h_\kappa^{2\min(n,p_{a,\kappa}+1)-2}}{p_{a,\kappa}^{2n-3}}\left(\|\mathscr{E}\ddot{\varphi}\|_{n,\mathcal{K}}^2+\|\mathscr{E}\dot{\varphi}\|_{n,\mathcal{K}}^2+\|\mathscr{E}\varphi\|_{n,\mathcal{K}}^2\right)\Bigg)\mathrm{d}\tau.$$

Whenever the meshsize is quasi-uniform, i.e. $h\simeq h_\kappa\,\forall\kappa\in\mathcal{T}_h$, the polynomial degree distribution is uniform, i.e. $p_{e,\kappa}=p_e\,\forall\kappa\in\mathcal{T}_h^e$ and $p_{a,\kappa}=p_a\,\forall\kappa\in\mathcal{T}_h^a$, and the solution is sufficiently regular, the above result reads as follows.

Corollary 7.2 (*A priori* error estimate in the energy norm)**.** *Under the hypotheses of Theorem 7.1, assume moreover that $h\simeq h_\kappa$ for any $\kappa\in\mathcal{T}_h$, $p_{e,\kappa}=p_e$ for any $\kappa\in\mathcal{T}_h^e$, and $p_{a,\kappa}=p_a$ for any $\kappa\in\mathcal{T}_h^a$. Then, if $(\mathbf{u},\varphi)\in C^2([0,T];\mathbf{H}^m(\Omega_e))\times C^2([0,T];H^n(\Omega_a))$ with $m\geqslant p_e+1$ and $n\geqslant p_a+1$, the error estimate (25) reads*

$$\sup_{t\in[0,T]}\|\mathbf{E}(t)\|_{\mathcal{E}}^2\lesssim\frac{h^{2p_e}}{p_e^{2m-3}}\left(\sup_{t\in[0,T]}\left(\|\dot{\mathbf{u}}\|_{m,\Omega_e}^2+\|\mathbf{u}\|_{m,\Omega_e}^2\right)+\int_0^T\left(\|\ddot{\mathbf{u}}\|_{m,\Omega_e}^2+\|\dot{\mathbf{u}}\|_{m,\Omega_e}^2+\|\mathbf{u}\|_{m,\Omega_e}^2\right)\mathrm{d}t\right)$$
$$+\frac{h^{2p_a}}{p_a^{2n-3}}\left(\sup_{t\in[0,T]}\left(\|\dot{\varphi}\|_{n,\Omega_a}^2+\|\varphi\|_{n,\Omega_a}^2\right)+\int_0^T\left(\|\ddot{\varphi}\|_{n,\Omega_a}^2+\|\dot{\varphi}\|_{n,\Omega_a}^2+\|\varphi\|_{n,\Omega_a}^2\right)\mathrm{d}t\right). \tag{26}$$

8. Fully discrete formulation

With a view towards writing the semi-discrete algebraic formulation of the problem, we fix a basis to span the discrete spaces $\mathbf{V}_h^e$ and V_h^a (cf. Section 9 for details). The semi-discrete algebraic formulation of (16) then reads

$$\begin{cases}\mathsf{M}_e^1\ddot{\mathsf{U}}(t)+\mathsf{M}_e^2\dot{\mathsf{U}}(t)+(\mathsf{M}_e^3+\mathsf{A}_e)\mathsf{U}(t)+\mathsf{C}_e\dot{\mathsf{\Phi}}(t)=\mathsf{F}_e(t), & t\in(0,T],\\ \mathsf{M}_a\ddot{\mathsf{\Phi}}(t)+\mathsf{A}_a\mathsf{\Phi}(t)+\mathsf{C}_a\dot{\mathsf{U}}(t)=\mathsf{F}_a(t), & t\in(0,T],\\ \mathsf{U}(0)=\mathsf{U}^0,\\ \dot{\mathsf{U}}(0)=\mathsf{V}^0,\\ \mathsf{\Phi}(0)=\mathsf{\Phi}^0,\\ \dot{\mathsf{\Phi}}(0)=\mathsf{\Psi}^0,\end{cases} \tag{27}$$

where vectors $\mathsf{U}(t)$ and $\mathsf{\Phi}(t)$ represent the expansion coefficients of $\boldsymbol{u}_h(t)$ and $\varphi_h(t)$ in the chosen bases. Analogously, M_e^1, M_e^2, M_e^3, A_e, and C_e are the matrices stemming from the bilinear forms

$$(\rho_e\mathbf{u},\mathbf{v})_{\Omega_e},\ (2\rho_e\zeta\mathbf{u},\mathbf{v})_{\Omega_e},\ (\rho_e\zeta^2\mathbf{u},\mathbf{v})_{\Omega_e},\ \mathcal{A}_h(\mathbf{u},\mathbf{v}),\ \mathcal{I}_h^e(\psi,\mathbf{v}),$$

respectively, and M_a, A_a, $\mathsf{C}_a \equiv -\mathsf{C}_e^{\mathsf{T}}$ represent the bilinear forms

$$(c^{-2}\rho_a\varphi,\psi)_{\Omega_a},\ \mathcal{A}_h^a(\varphi,\psi),\ \mathcal{I}_h^a(\mathbf{v},\psi),$$

respectively. Finally, $\mathsf{F}_e(t)$ and $\mathsf{F}_a(t)$ are the vector representations of linear functionals $(\mathbf{f}_e(t),\mathbf{v})_{\Omega_e}$ and $(\rho_a f_a(t),\psi)_{\Omega_a}$, respectively.

To fully discretize (16), we employ a time marching method based on centered finite-difference, widely employed for the numerical simulation of wave propagation, namely, the *leap-frog* scheme. We now subdivide the time interval $[0,T]$ into N_T subintervals of amplitude $\Delta t = T/N_T$ and we denote by $\mathsf{U}^i \approx \mathsf{U}(t_i)$ and $\mathsf{\Phi}^i \approx \mathsf{\Phi}(t_i)$ the approximations of U and $\mathsf{\Phi}$ at time $t_i = i\Delta t$, $i \in \{1,\dots,N_T\}$. The leap-frog (centered finite-difference) method reads then

$$\begin{bmatrix} \mathsf{M}_e^1 + \frac{\Delta t}{2}\mathsf{M}_e^2 & \frac{\Delta t}{2}\mathsf{C}_e \\ -\frac{\Delta t}{2}\mathsf{C}_e^{\mathsf{T}} & \mathsf{M}_a \end{bmatrix} \begin{bmatrix} \mathsf{U}^{n+1} \\ \mathsf{\Phi}^{n+1} \end{bmatrix} = \begin{bmatrix} -\mathsf{M}_e^1 + \frac{\Delta t}{2}\mathsf{M}_e^2 & \frac{\Delta t}{2}\mathsf{C}_e \\ -\frac{\Delta t}{2}\mathsf{C}_e^{\mathsf{T}} & -\mathsf{M}_a \end{bmatrix} \begin{bmatrix} \mathsf{U}^{n-1} \\ \mathsf{\Phi}^{n-1} \end{bmatrix} + \begin{bmatrix} 2\mathsf{M}_e^1 - \Delta t^2(\mathsf{A}_e + \mathsf{M}_e^3) & 0 \\ 0 & 2\mathsf{M}_a - \Delta t^2 \mathsf{A}_a \end{bmatrix} \begin{bmatrix} \mathsf{U}^n \\ \mathsf{\Phi}^n \end{bmatrix} + \Delta t^2 \begin{bmatrix} \mathsf{F}_e^n \\ \mathsf{F}_a^n \end{bmatrix}, \tag{28}$$

for $n \in \{1,\dots,N_T-1\}$, and

$$\begin{aligned} \mathsf{M}_e^1\mathsf{U}^1 &= \left(\mathsf{M}_e^1 - \frac{\Delta t^2}{2}(\mathsf{A}_e + \mathsf{M}_e^3)\right)\mathsf{U}^0 + \Delta t(\mathsf{M}_e^1 - \mathsf{M}_e^2)\mathsf{V}^0 - \frac{\Delta t^2}{2}\mathsf{C}_e\mathsf{\Psi}^0 + \frac{\Delta t^2}{2}\mathsf{F}_e^0, \\ \mathsf{M}_a\mathsf{\Phi}^1 &= \left(\mathsf{M}_a - \frac{\Delta t^2}{2}\mathsf{A}_a\right)\mathsf{\Phi}^0 + \Delta t\mathsf{M}_a\mathsf{\Psi}^0 + \frac{\Delta t^2}{2}\mathsf{C}_e^{\mathsf{T}}\mathsf{V}^0 + \frac{\Delta t^2}{2}\mathsf{F}_a^0, \end{aligned}$$

with $\mathsf{F}_{e(a)}^i = \mathsf{F}_{e(a)}(t_i)$, $i \in \{0,\dots,N_T-1\}$. Let us remark that the centered finite-difference method is an explicit second-order-accurate scheme; thus, to ensure its numerical stability, a Courant-Friedrich-Lewy (CFL) condition has to be satisfied (see [73]). In particular, when uniform meshsizes h_e and h_a and uniform polynomial degrees p_e, p_a are used, the CFL condition reads

$$\Delta t \leqslant C_{\text{cfl}} \min\left(\frac{h_e}{p_e^2 c_P}, \frac{h_a}{p_a^2 c}\right), \tag{29}$$

where $C_{\text{cfl}} \in (0,1)$ (see also [12] for the purely elastic case).

9. Benchmark test cases

In this section we solve problem (1) in the rectangle $\Omega = (-1,1)\times(0,1)$ on polygonal meshes such as the one represented in Figure 5. Numerical experiments have been carried out both to test *hp*-convergence (besides validating numerically estimate (26) by computing the dG-norm of the error, we also check convergence of the method in the L^2-norm) and to simulate a problem of physical interest, where the system is excited by a point source load in the acoustic domain. In all cases, we assume that $\Omega_e = (-1,0)\times(0,1)$ is occupied by a homogeneous and isotropic material, and $\Omega_a = (0,1)\times(0,1)$ is occupied by a fluid with constant density ρ_a. The interface is given by $\Gamma_{\text{I}} = \{0\}\times(0,1)$. Meshes have been generated using `PolyMesher` [74]. The timestep will be precised depending on the case under consideration. In all of the numerical experiments of

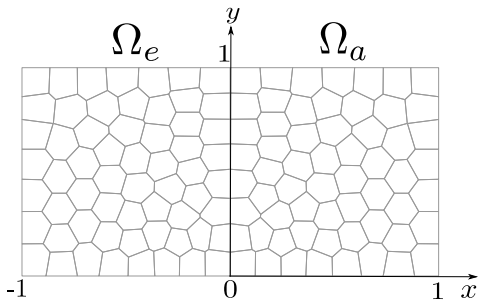

Figure 5: Computational domain and mesh made up by 120 polygons.

this section, as in [9, 47], we choose the following values of the material parameters: $c_P = 6.20$, $c_S = 3.12$, $\rho_e = 2.7$, $\rho_a = 1$, and $c = 1$.

Concerning the choice of the basis to span the finite-dimensional spaces, along the lines of [19, Section 6.3] to which we refer the reader for a comprehensive and detailed presentation, we employ the so called "bounding box" approach, based on employing suitably scaled and cropped tensor-product Legendre polynomials of total degree at most p_κ on each mesh element $\kappa \in \mathcal{T}_h$.

9.1. Test case 1

In this test case, the right-hand sides $\mathbf{f}_e$ and f_a are chosen so that the exact solution is given by

$$\mathbf{u}(x,y;t) = x^2 \cos(\sqrt{2}\pi t) \cos\left(\frac{\pi}{2}x\right) \sin(\pi y)\, \hat{\mathbf{u}}, \quad \varphi(x,y;t) = x^2 \sin(\sqrt{2}\pi t) \sin(\pi x) \sin(\pi y), \tag{30}$$

where $\hat{\mathbf{u}} = (1,1)$. The timestep is here set to $\Delta t = 10^{-4}$, so that the error due to time integration is negligeable, and the final time is set to $T = 1$. Notice that, in this case, both the left- and right-hand sides of the transmission conditions on Γ_{I} (cf. (1)) vanish, as well as the unknowns $\mathbf{u}$ and φ themselves. Figure 6 shows convergence results in the dG- and L^2-norms respectively, for four nested, sequentially refined polygonal meshes, when polynomials of uniform degree $p_e = p_a \equiv p = 2$ are employed. The numerical results concerning the dG-error show asymptotic convergence rates that match those predicted by estimate (26). Also, as it is typical for dG methods, the L^2-error turns out to converge in h^{p+1} (see, e.g., [72, Theorem 2] for the case of the elastodynamics equation).

Figure 7 shows convergence results in a semilogarithmic scale, in the dG- and L^2-norms respectively, for a fixed mesh given by 300 elements and a uniform polynomial degree ranging from 1 to 5. Since the exact solution is analytical, as expected, the error undergoes an exponential decay.

9.2. Test case 2

We now choose the right-hand sides $\mathbf{f}_e$ and f_a so that the exact solution is given by

$$\mathbf{u}(x,y;t) = \left(\cos\left(\frac{4\pi x}{c_P}\right), \cos\left(\frac{4\pi x}{c_S}\right)\right) \cos(4\pi t), \quad \varphi(x,y;t) = \sin\left(\frac{4\pi x}{c}\right) \sin(4\pi t). \tag{31}$$

The same test has been carried out in [9] using a Spectral Element discretization; the choice of material parameters is also the same as in the previous test case. In this case, on Γ_{I}, both

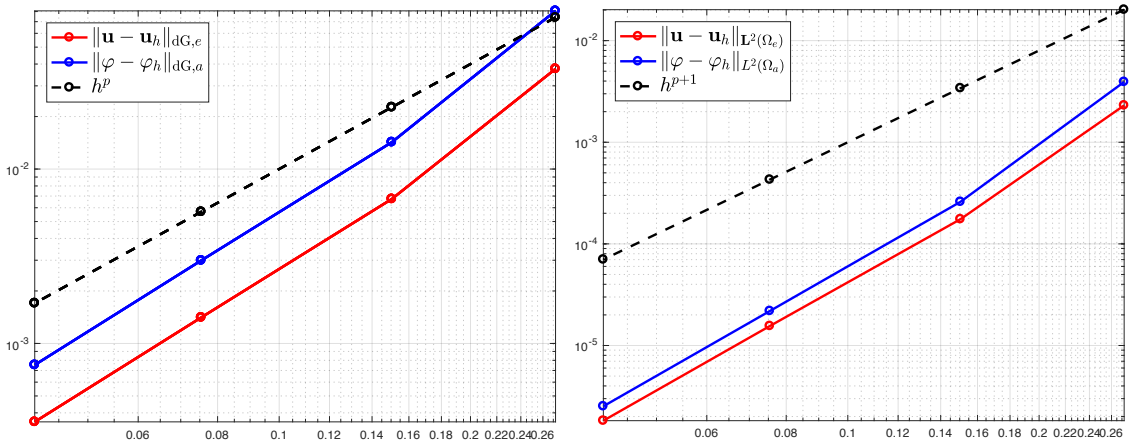

(a) $\|\mathbf{u}-\mathbf{u}_h\|_{\mathrm{dG},e}$ and $\|\varphi-\varphi_h\|_{\mathrm{dG},a}$ vs. h at $T=1$ (b) $\|\mathbf{u}-\mathbf{u}_h\|_{\Omega_e}$ and $\|\varphi-\varphi_h\|_{\Omega_a}$ vs. h at $T=1$

Figure 6: Test case 1. dG-error and L^2-error vs. h for four sequentially refined polygonal meshes and second-order polynomials ($p_e = p_a \equiv p = 2$).

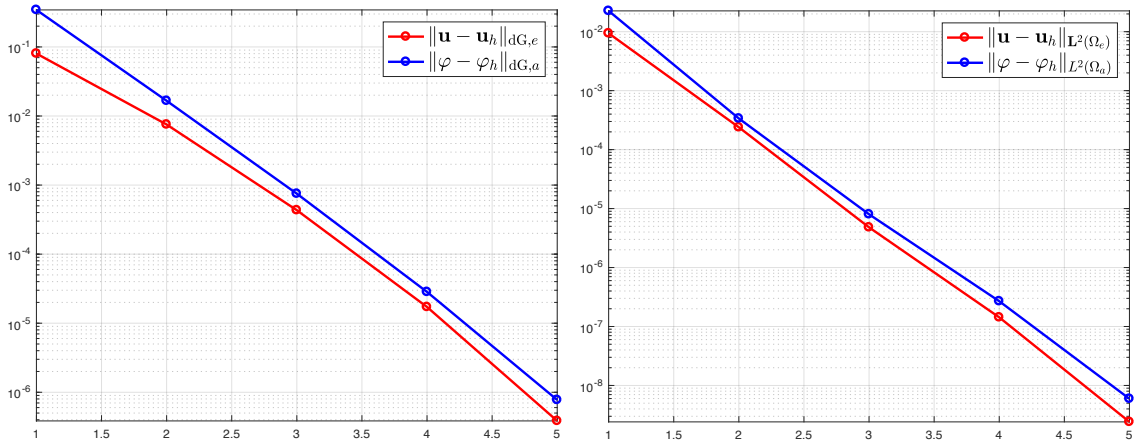

(a) $\|\mathbf{u}-\mathbf{u}_h\|_{\mathrm{dG},e}$ and $\|\varphi-\varphi_h\|_{\mathrm{dG},a}$ vs. p at $T=1$ (b) $\|\mathbf{u}-\mathbf{u}_h\|_{\Omega_e}$ and $\|\varphi-\varphi_h\|_{\Omega_a}$ vs. p at $T=1$

Figure 7: Test case 1. dG-error and L^2-error vs. p for $p_e = p_a \equiv p$ ranging from 1 to 5 and a mesh given by 300 polygons.

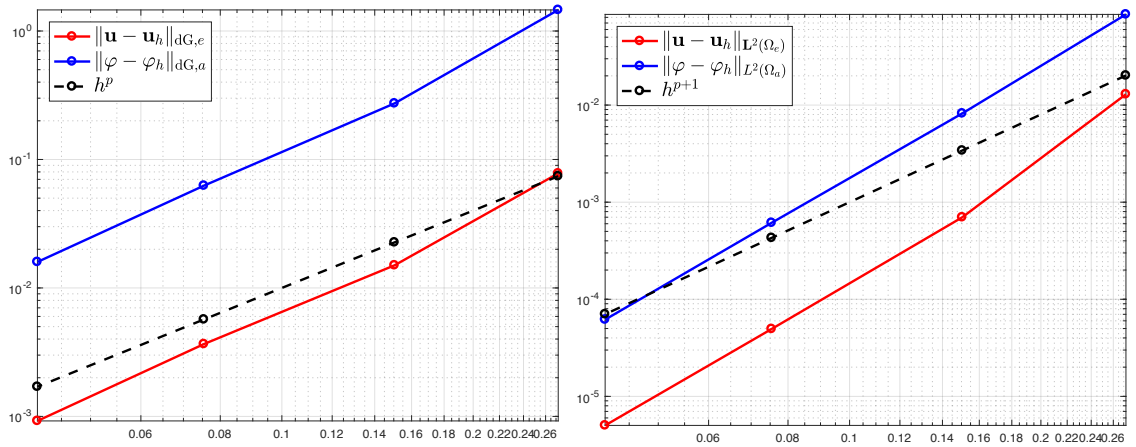

(a) $\|\mathbf{u}-\mathbf{u}_h\|_{\mathrm{dG},e}$ and $\|\varphi-\varphi_h\|_{\mathrm{dG},a}$ vs. h at $T=0.8$ (b) $\|\mathbf{u}-\mathbf{u}_h\|_{\Omega_e}$ and $\|\varphi-\varphi_h\|_{\Omega_a}$ vs. h at $T=0.8$

Figure 8: Test case 2. dG-error and L^2-error vs. h for four sequentially refined polygonal meshes and second-order polynomials ($p_e=p_a\equiv p=2$).

the traction $\boldsymbol{\sigma}(\mathbf{u})\mathbf{n}_e$ and the acoustic pressure $-\rho_a\dot{\varphi}\mathbf{n}_e$ vanish; on the other hand, we have $\partial\varphi/\partial\mathbf{n}_a=-\dot{\mathbf{u}}\cdot\mathbf{n}_a=4\pi\sin(4\pi t)$. The timestep is, again, set to $\Delta t=10^{-4}$; on the other hand, the final time is in this case set to $T=0.8$, to ensure that none of the two unknowns $\mathbf{u}$ and φ be identically zero when dG- and L^2-errors are computed.

Figure 8 shows convergence results in the dG- and L^2-norms respectively, for four nested, sequentially refined polygonal meshes, when polynomials of uniform degree $p_e=p_a\equiv p=2$ are employed. The numerical results concerning the dG-error again show asymptotic convergence rates matching those predicted by estimate (26). Also, notice that the L^2-error convergence rates turn out to be slightly above the optimal rate h^{p+1} both for $\mathbf{u}$ and for φ; in the latter case, this difference is more remarkable. This behavior is probably due to the observation time T at which the errors are computed (see also [75]); indeed, if we consider $T=0.0625$, the convergence rate of the L^2-error is closer to the optimal rate h^{p+1} (cf. Figure 9).

Figure 10 shows convergence results in a semilogarithmic scale, in the dG- and L^2-norms respectively, for a fixed mesh given by 300 elements and a uniform polynomial degree ranging from 1 to 5. Again, the error undergoes an exponential decay. Notice that, concerning the L^2-error on $\mathbf{u}$ (Figure 10b), the convergence rate decreases when passing from polynomial degree 4 to 5: in both cases the L^2-error is on the order of 10^{-7}. This behavior is related to the choice of the timestep Δt, set to 10^{-4}; indeed, when a leap-frog time discretization is employed, the error is expected to converge in Δt^2. In our case, $\Delta t^2=10^{-8}$, which is only one order of magnitude lower than the L^2-error for $p=4$ and $p=5$. Decreasing the timestep to $\Delta t=10^{-5}$ allows to recover the expected convergence.

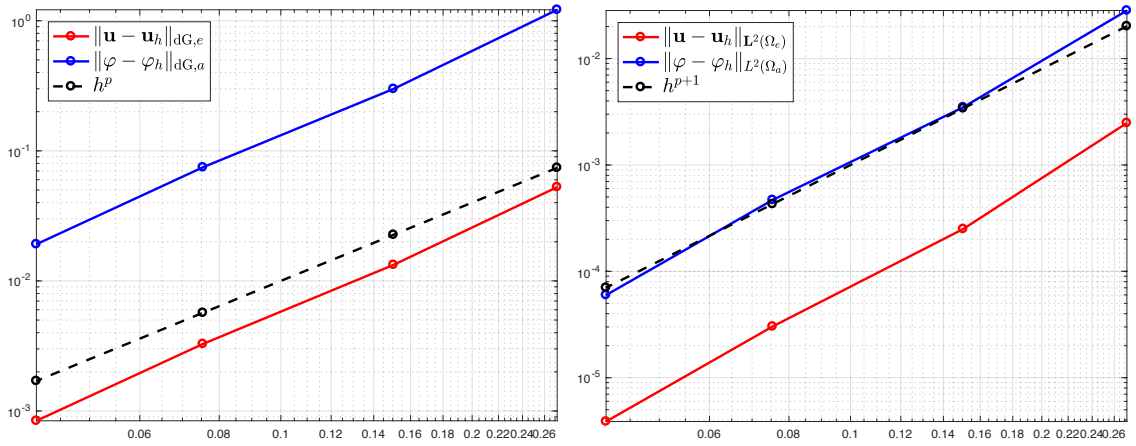

(a) $\|\mathbf{u}-\mathbf{u}_h\|_{\mathrm{dG},e}$ and $\|\varphi-\varphi_h\|_{\mathrm{dG},a}$ vs. h at $T = 0.0625$ (b) $\|\mathbf{u}-\mathbf{u}_h\|_{\Omega_e}$ and $\|\varphi-\varphi_h\|_{\Omega_a}$ vs. h at $T = 0.0625$

Figure 9: Test case 2. dG-error and L^2-error vs. h for four sequentially refined polygonal meshes and second-order polynomials ($p_e = p_a \equiv p = 2$).

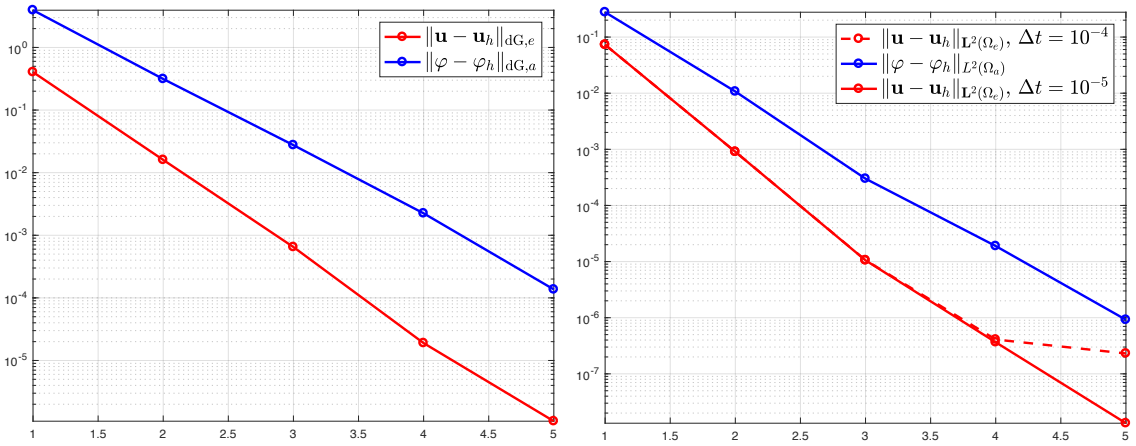

(a) $\|\mathbf{u}-\mathbf{u}_h\|_{\mathrm{dG},e}$ and $\|\varphi-\varphi_h\|_{\mathrm{dG},a}$ vs. p at $T = 0.8$ (b) $\|\mathbf{u}-\mathbf{u}_h\|_{\Omega_e}$ and $\|\varphi-\varphi_h\|_{\Omega_a}$ vs. p at $T = 0.8$

Figure 10: Test case 2. dG-error and L^2-error vs. p for $p_e = p_a \equiv p$ ranging from 1 to 5 and a mesh given by 300 polygons.

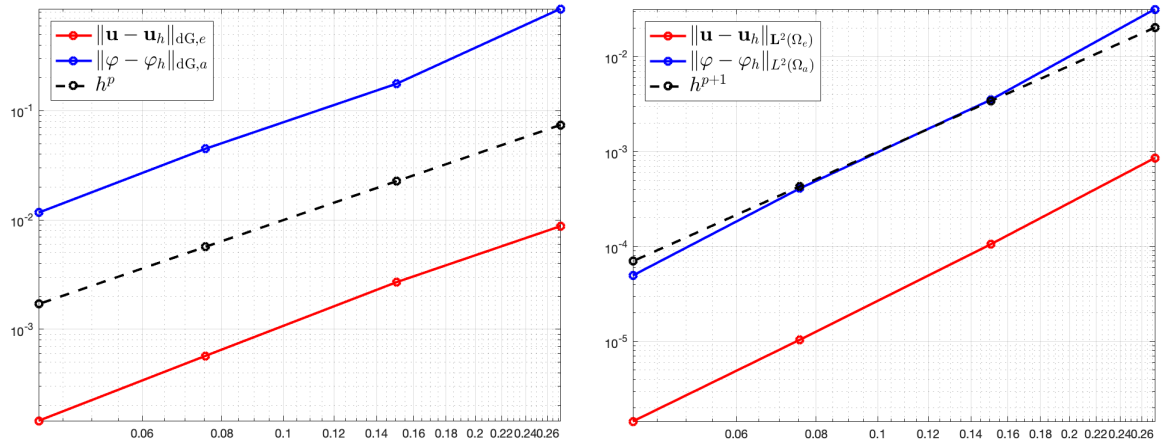

(a) $\|\mathbf{u}-\mathbf{u}_h\|_{\mathrm{dG},e}$ and $\|\varphi-\varphi_h\|_{\mathrm{dG},a}$ vs. h at $T=1$ (b) $\|\mathbf{u}-\mathbf{u}_h\|_{\Omega_e}$ and $\|\varphi-\varphi_h\|_{\Omega_a}$ vs. h at $T=1$

Figure 11: Test case 3. dG-error and L^2-error vs. h for four sequentially refined polygonal meshes and second-order polynomials ($p_e = p_a \equiv p = 2$).

9.3. Test case 3 – nonzero damping

We now consider a test case where $\zeta \neq 0$ (in particular, we set $\zeta = 4\pi$), and choose the right-hand sides $\mathbf{f}_e$ and f_a so that the exact solution is given by

$$\mathbf{u}(x,y;t) = \left(\cos\left(\frac{4\pi x}{c_P}\right), \cos\left(\frac{4\pi x}{c_S}\right)\right) e^{-4\pi t}, \quad \varphi(x,y;t) = \sin\left(\frac{4\pi x}{c}\right) e^{-4\pi t}. \tag{32}$$

Concerning the transmission conditions on Γ_{I}, the situation is completely analogous to Test case 2. The timestep is set to $\Delta t = 10^{-5}$, and the final time is set to $T = 1$.

Figure 11 (resp. Figure 12) shows the computed errors in the dG- and L^2-norms respectively, for four nested, sequentially refined polygonal meshes, when polynomials of uniform degree $p_e = p_a = 2$ (resp. $p_e = p_a = 3$) are employed. The numerical results concerning the dG-error again show asymptotic convergence rates matching those predicted by estimate (26).

Finally, Figure 13 shows an exponential rate of convergence of the error measured in the dG- and L^2-norms respectively, for a fixed mesh given by 300 elements and a uniform polynomial degree ranging from 1 to 5. The error undergoes an exponential decay as expected.

Notice that, in all of the numerical experiments carried out in this section, the h^{p+1}-convergence of the L^2-error resulting from h-refinement and its exponential convergence resulting from p-refinements is in agreement with the numerical results available in the literature (see e.g. [47, 49]).

To close this section, we give an insight into the computational costs of our method. More precisely, in Table 1 we report the sizes of the matrix to be inverted at each time-step in the left-hand side of (28), the number of its nonzero elements, and the ratio of the latter with respect to the former, for $p_e = p_a \equiv p \in \{2, 3\}$ and a sequence of four sequentially refined polygonal meshes. We recall that for the solution of (28) we employ a direct solver based on the LU factorization; notice that $\mathsf{M}_{\mathsf{e}}^1$, M_e^2, and M_a are block diagonal. Thus, the amount of time spent for a single step is negligeable with respect to the one spent for the assembly of the matrix.

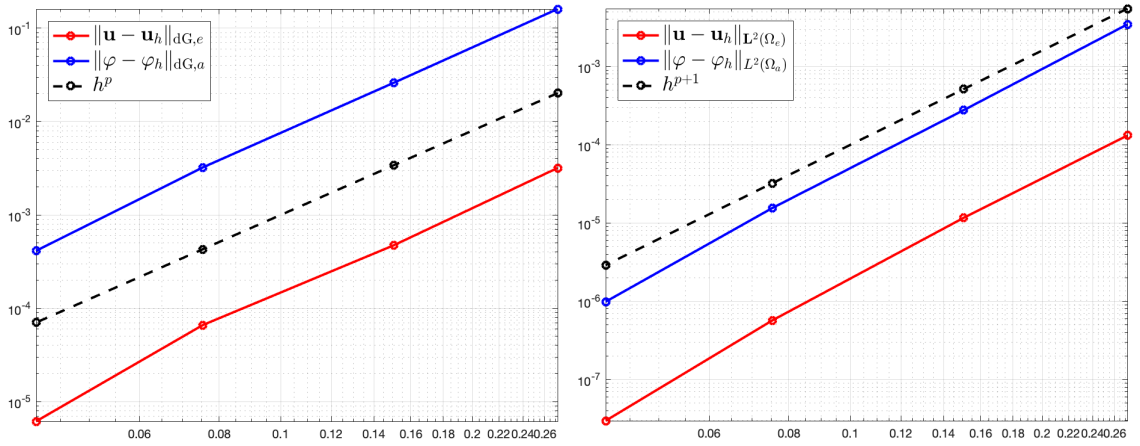

(a) $\|\mathbf{u}-\mathbf{u}_h\|_{\mathrm{dG},e}$ and $\|\varphi-\varphi_h\|_{\mathrm{dG},a}$ vs. h at $T=1$ (b) $\|\mathbf{u}-\mathbf{u}_h\|_{\Omega_e}$ and $\|\varphi-\varphi_h\|_{\Omega_a}$ vs. h at $T=1$

Figure 12: Test case 3. dG-error and L^2-error vs. h for four sequentially refined polygonal meshes and third-order polynomials ($p_e = p_a \equiv p = 3$).

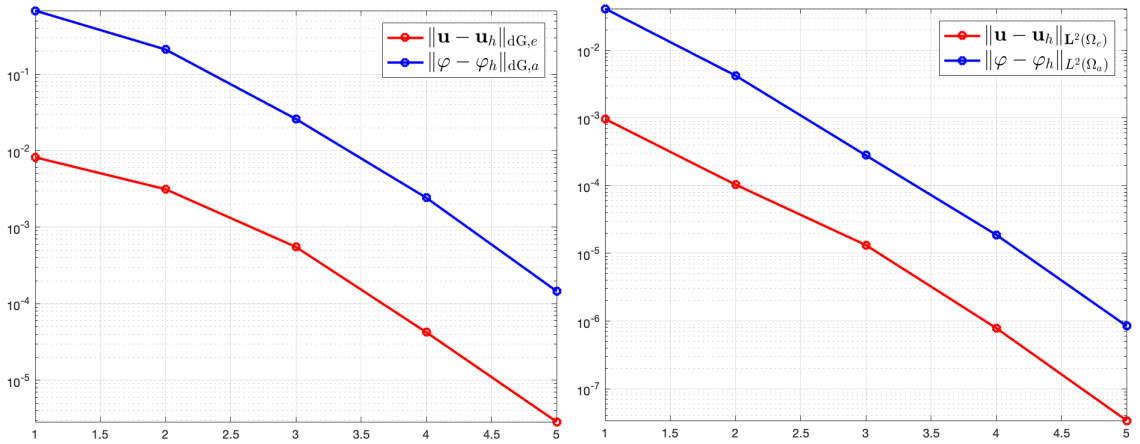

(a) $\|\mathbf{u}-\mathbf{u}_h\|_{\mathrm{dG},e}$ and $\|\varphi-\varphi_h\|_{\mathrm{dG},a}$ vs. p at $T=1$ (b) $\|\mathbf{u}-\mathbf{u}_h\|_{\Omega_e}$ and $\|\varphi-\varphi_h\|_{\Omega_a}$ vs. p at $T=1$

Figure 13: Test case 3. dG-error and L^2-error vs. p for $p_a = p_e \equiv p$ ranging from 1 to 5 and a mesh given by 300 polygons.

	$p=2$				$p=3$			
$\mathrm{N_{el}}$	80	320	1280	5120	80	320	1280	5120
S	720	2880	11520	46080	1200	4800	19200	76800
NNZ	4824	18648	71552	282046	13392	51756	198778	783518
$\mathrm{NNZ/S^2}$	9e-3	2e-3	5e-4	1e-4	9e-3	2.2e-3	5e-4	1e-4

Table 1: Computational costs of the method in terms of the nonzero elements of the matrix to be inverted at each time-step for $p_e = p_a \equiv p \in \{2, 3\}$, using a sequence of four sequentially refined polygonal grids. $\mathrm{N_{el}}$ = number of polygons in each grid, S = size of the matrix, NNZ = number of nonzero elements of the matrix.

10. Physical examples

10.1. Acoustic point source

As a first numerical experiment, we simulate a seismic source. In particular, we suppose that the system is excited *only* by a Ricker wavelet [76], i.e., by the following point source load placed in the acoustic domain:

$$f_a(\mathbf{x},t) = f_0\left(1-2\pi^2 f_p^2(t-t_0)^2\right)e^{-\pi^2 f_p^2(t-t_0)^2}\delta(\mathbf{x}-\mathbf{x}_0), \quad \mathbf{x}_0\in\Omega_a,\ t_0\in(0,T], \tag{33}$$

where $\mathbf{x}\equiv(x,y)$, $\mathbf{x}_0\equiv(x_0,y_0)$ is a given point in Ω_a, δ is the Dirac distribution, f_0 represents the intensity of the source, and f_p is the peak frequency. All initial conditions, boundary conditions, as well as the body force $\mathbf{f}_e$, are set to zero. The Dirac distribution in $\mathbf{x}_0$ is approximated numerically by a Gaussian distribution centered at $\mathbf{x}_0$. The computational domain is the same as in the previous section, where the length and width are measured in cm and the elastic medium is again homogeneous and isotropic. For the material parameters, we consider here the same numerical values as in [47], namely, $\rho_e = 2.5\,g/cm^3$, $\rho_a = 1\,g/cm^3$, $c_P = 4.0\,cm/s$, $c_S = 2.0\,cm/s$, $c = 1.5\,cm/s$, and we assume a zero damping, i.e. $\zeta = 0$. Moreover, in (33), we choose $\mathbf{x}_0 = (0.2\,cm, 0.5\,cm)$, $t_0 = 0.1\,s$, and, as in [47], $f_0 = 3620\,Hz\cdot cm^3$ and $f_p = 13.5\,Hz$. We employ here a polygonal mesh of 5000 elements, corresponding to a meshsize $h \simeq 0.04$, a uniform polynomial degree $p = 3$, and a timestep $\Delta t = 10^{-5}\,s$. The final time is set to $T = 1\,s$.

Figure 14 shows the numerical solution (horizontal and vertical elastic displacements, and acoustic potential) at time $t = 0.5\,s$. The vertical displacement, displayed in Figure 14b, turns out to be very close to zero in a large elastic subregion, except near the boundary, where small reflected wavefronts can be detected, because of homogeneous Dirichlet boundary conditions. This behavior is due to the fact that the seismic source is placed close enough to the interface Γ_I, so that the effects of reflected waves in the elastic region are not observed for a certain time, and hence only the coupling effects are visible (only longitudinal stresses are propagated through the elasto-acoustic interface, since fluids cannot sustain shear stresses). Nevertheless, after a certain time, elastic waves are reflected, which gives rise to a nonzero vertical displacement. Concerning the acoustic region, spherical wavefronts generated by the point source load can be clearly observed in Figure 14c; again, waves are reflected on the boundary for the same reason as before.

10.2. Elastic point source in the presence of acoustic cavities

To further demonstrate the effectiveness of our approach in the simulation of elasto-acoustic coupling, we now consider the situation of a $100\,m \times 100\,m$ elastic square domain including 45 acoustic cavities. Each acoustic cavity is itself a polygonal element of the mesh (cf. Figure 15), which is made up overall by 4861 elements, resulting in a meshsize $h \simeq 10.45\,m$. We simulate the effect of a seismic source acting in the elastic domain and located at point $\mathbf{x}_0 = (10\,m, 10\,m)$; the time factor is the same as in Section 10.1, with $f_0 = 10^4\,N$, $f_p = 1\,Hz$, and $t_0 = 2\,s$. Initial conditions, boundary conditions, and the acoustic source f_a are all set to zero. The elastic medium is homogeneous and isotropic, and is characterized by a density $\rho_e = 1600\,kg/m^3$ and by wave propagation velocities $c_P = 25\,m/s$ and $c_S = 10\,m/s$, resulting in the following values of the Lamé parameters: $\lambda = 680\,kPa$ and $\mu = 160\,kPa$. On the other hand, we consider the air as acoustic medium, and thus set $\rho_a = 1000\,kg/m^3$ and $c = 300\,m/s$. We use on every mesh

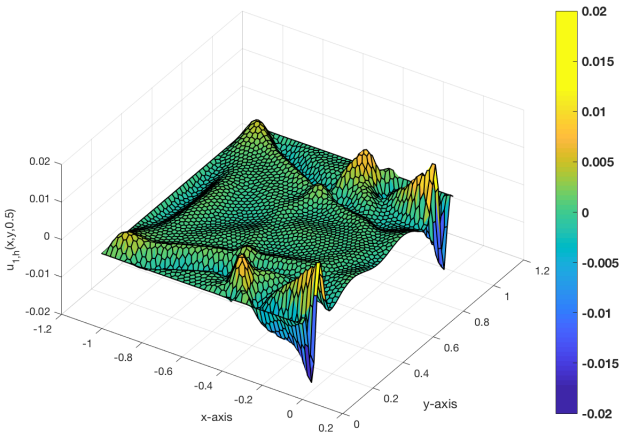

(a) Acoustic point source – Horizontal elastic displacement at $t = 0.5$

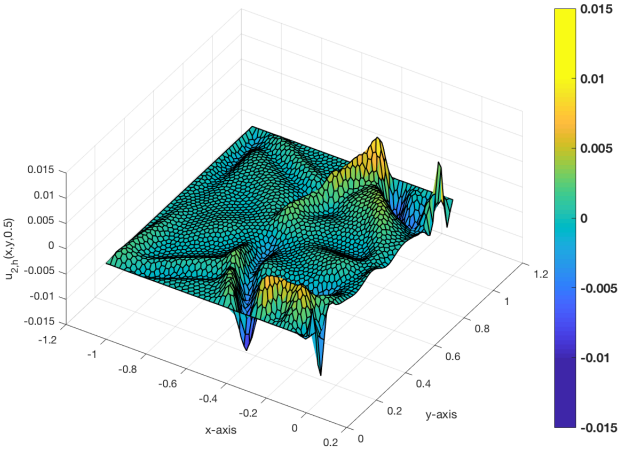

(b) Acoustic point source – Vertical elastic displacement at $t = 0.5$

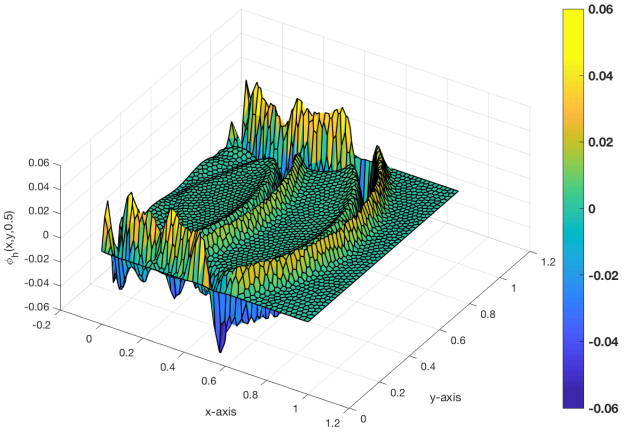

(c) Acoustic point source – Acoustic potential at $t = 0.5$

Figure 14: Numerical solution at $t = 0.5$.

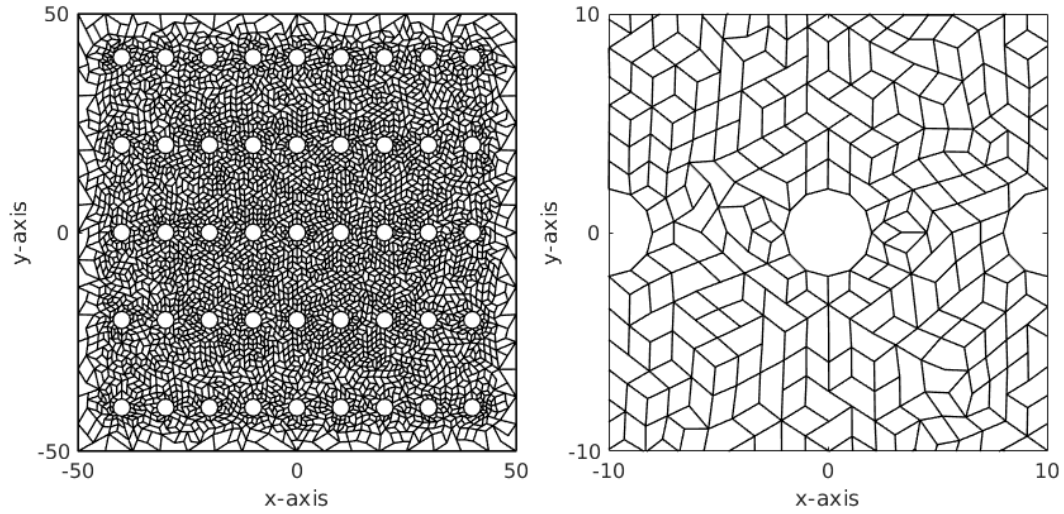

(a) (b)

Figure 15: Mesh of a $100\,m \times 100\,m$ elastic square domain with 45 acoustic cavities (a) and zoom on the neighborhood of an acoustic cavity (b). Each acoustic cavity is described by one single polygonal element with many faces.

element a polynomial degree $p = 3$, the time-step is $\Delta t = 10^{-4}\,s$, and the final time is set to $T = 10\,s$.

Figures 16 and 17 show the euclidean norm of the displacement field and the absolute value of the acoustic potential, respectively, at four different istants of time. The elastic wave gets scattered due to the presence of the acoustic inclusions and is reflected on the boundary due to homogeneous boundary conditions. On the other hand, the acoustic waves generated within the cavities are subject to refraction and reflection phenomena when interacting with the elastic domain.

11. Conclusions

We proposed and analyzed a high-order discontinuous Galerkin method for the approximation of a coupled elasto-acoustic evolution problem on computational meshes made by general polygonal/polyhedral elements. We established the well-posedness of the problem in the continuous setting based on the Hille–Yosida theory and we then analyzed the well-posedness of the semi-discrete formulation by stating and proving a stability result, as well as a *hp*-version error estimate for the semi-discrete problem. The proposed spatial discretization scheme features the following advantages: (i) grids on the elastic and acoustic domains can be generated independently, which allows for geometric flexibility; (ii) it allows for *hp*-tuning of discretization parameters; (iii) it is well-suited for applications (naturally oriented to high performance computing techniques). We have also discussed the fully discrete numerical scheme, based on the leap-frog method. Finally, we validated the theoretical results by numerical experiments carried out on several two-dimensional test cases. In particular, we carried out a simulation on a computational domain occupied by an elastic medium with several acoustic spherical inclusions. This

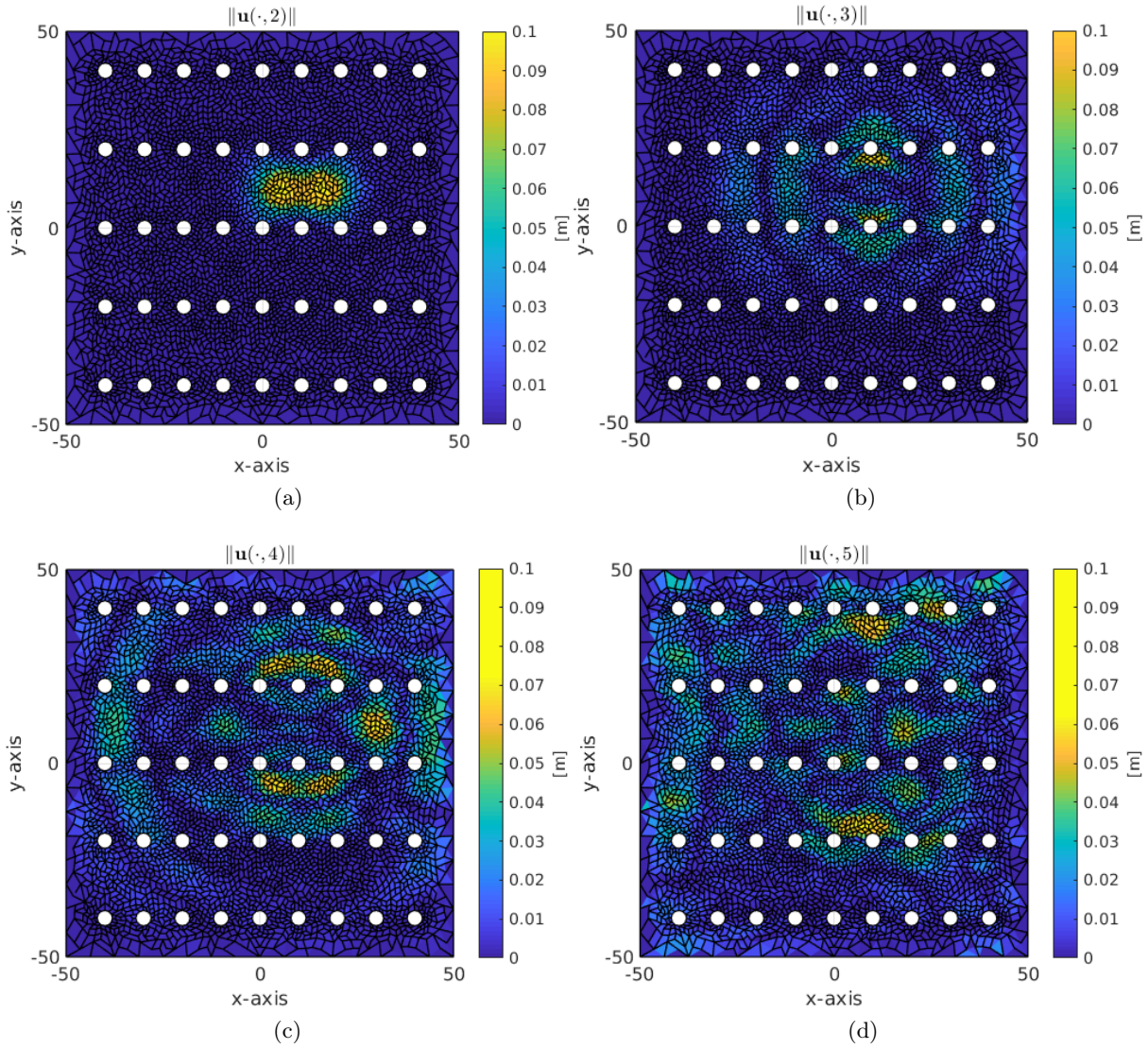

Figure 16: Euclidean norm of the displacement field at times $t = 2\,s$ (a), $t = 3\,s$ (b), $t = 4\,s$ (c), and $t = 5\,s$ (d).

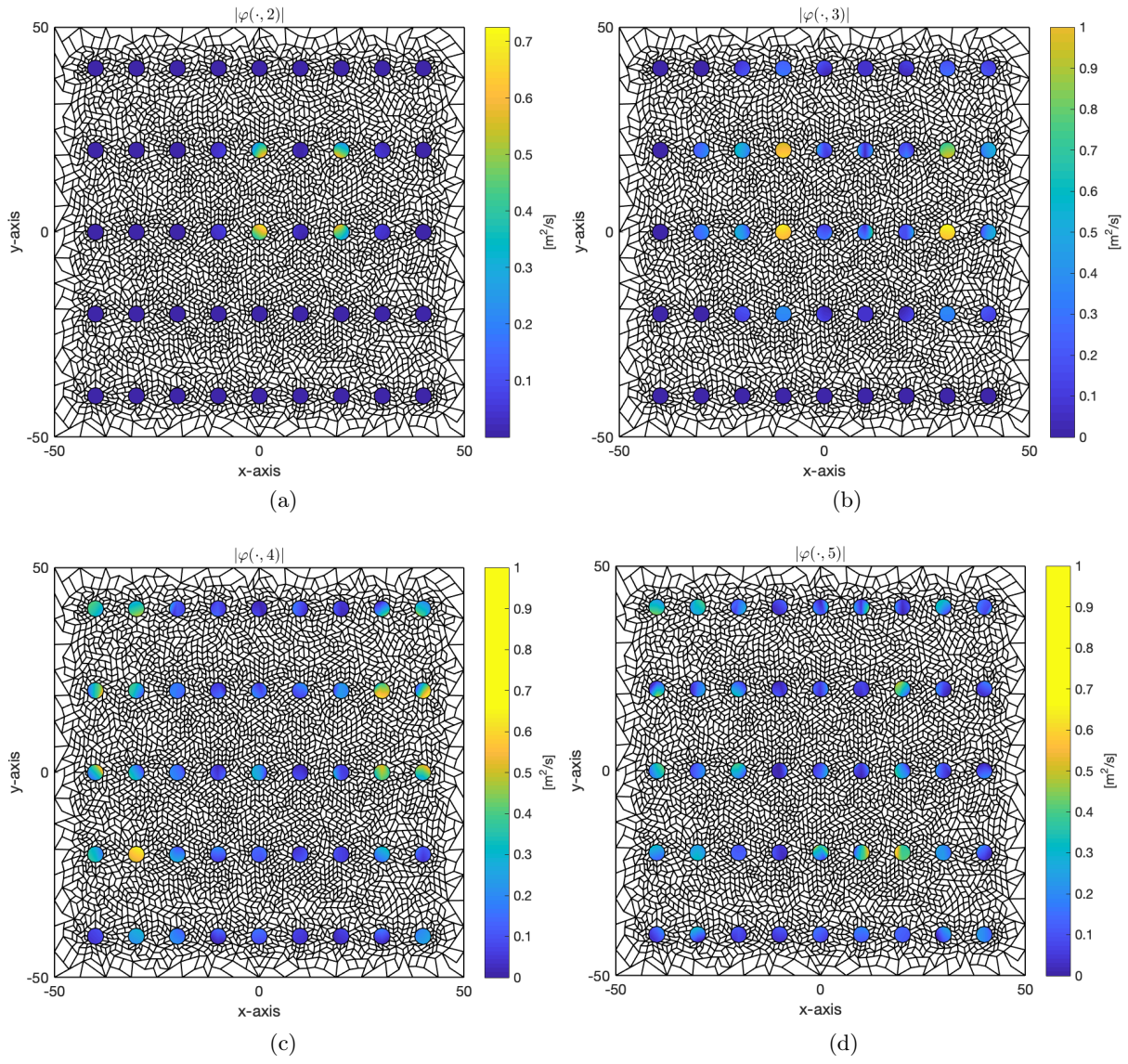

Figure 17: Absolute value of the acoustic potential at times $t = 2\,s$ (a), $t = 3\,s$ (b), $t = 4\,s$ (c), and $t = 5\,s$ (d).

test case shows that the flexibility in the process of mesh design offered by polytopic elements, can be fully exploited at a lower computational cost compared to conforming elements.

Appendix A.

The proofs of Theorems 3.1 (existence and uniqueness for the solution of the continuous problem), 6.2 (stability of the semi-discrete formulation), and 7.1 (semi-discrete error estimate), as well as the statements and proofs of Lemmas A.I and A.II, are presented here.

A.1. Existence and uniqueness

Proof of Theorem 3.1. Let $\mathbf{w} = \dot{\mathbf{u}}$, $\phi = \dot{\varphi}$, and $\mathcal{U} = (\mathbf{u}, \mathbf{w}, \varphi, \phi)$. We introduce the Hilbert space

$$\mathbb{H} = \mathbf{H}^1_D(\Omega_e) \times \mathbf{L}^2(\Omega_e) \times H^1_D(\Omega_a) \times L^2(\Omega_a),$$

equipped with the following scalar product:

$$\begin{aligned}(\mathcal{U}_1, \mathcal{U}_2)_{\mathbb{H}} = {} & (\rho_e \zeta^2 \mathbf{u}_1, \mathbf{u}_2)_{\Omega_e} + (\mathbb{C}\boldsymbol{\varepsilon}(\mathbf{u}_1), \boldsymbol{\varepsilon}(\mathbf{u}_2))_{\Omega_e} \\ & + (\rho_e \mathbf{w}_1, \mathbf{w}_2)_{\Omega_e} + (\rho_a \boldsymbol{\nabla}\varphi_1, \boldsymbol{\nabla}\varphi_2)_{\Omega_a} + (c^{-2}\rho_a \phi_1, \phi_2)_{\Omega_a}.\end{aligned} \tag{A.1}$$

Then, we define the operator $A\colon D(A) \subset \mathbb{H} \to \mathbb{H}$ by

$$A\mathcal{U} = \left(-\mathbf{w},\ 2\zeta\mathbf{w} + \zeta^2\mathbf{u} - \rho_e^{-1}\mathbf{div}\,\mathbb{C}\boldsymbol{\varepsilon}(\mathbf{u}),\ -\phi,\ -c^2\triangle\varphi\right) \quad \forall \mathcal{U} \in D(A),$$

where the domain $D(A)$ of the operator is the linear subspace of $\mathbb{H}$ defined as follows (cf. definition (3)):

$$\begin{aligned}D(A) = \Big\{ & \mathcal{U} \in \mathbb{H} : \mathbf{u} \in \mathbf{H}^{\triangle}_{\mathbb{C}}(\Omega_e),\ \mathbf{w} \in \mathbf{H}^1_D(\Omega_e),\ \varphi \in H^{\triangle}(\Omega_a),\ \phi \in H^1_D(\Omega_a); \\ & (\mathbb{C}\boldsymbol{\varepsilon}(\mathbf{u}) + \rho_a\phi\mathbf{I})\,\mathbf{n}_e = \mathbf{0} \text{ on } \Gamma_{\mathrm{I}},\quad (\boldsymbol{\nabla}\varphi + \mathbf{w})\cdot\mathbf{n}_a = 0 \text{ on } \Gamma_{\mathrm{I}}\Big\}.\end{aligned} \tag{A.2}$$

Finally, let

$$\mathcal{F} = (\mathbf{0}, \rho_e^{-1}\mathbf{f}_e, 0, c^2 f_a).$$

Problem (1) can then be reformulated as follows: given $\mathcal{F} \in C^1([0,T];\mathbb{H})$ and $\mathcal{U}_0 \in D(A)$, find $\mathcal{U} \in C^1([0,T];\mathbb{H}) \cap C^0([0,T];D(A))$ such that

$$\begin{aligned}\frac{\mathrm{d}\mathcal{U}}{\mathrm{d}t}(t) + A\mathcal{U}(t) &= \mathcal{F}(t), \quad t \in (0,T], \\ \mathcal{U}(0) &= \mathcal{U}_0.\end{aligned} \tag{A.3}$$

Owing to the Hille–Yosida Theorem, this problem is well-posed provided A is maximal monotone, i.e., $(A\mathcal{U}, \mathcal{U})_{\mathbb{H}} \geqslant 0\ \forall \mathcal{U} \in D(A)$ and $I + A$ is surjective from $D(A)$ onto $\mathbb{H}$. By the definition (A.1) of the scalar product in $\mathbb{H}$, we have

$$\begin{aligned}(A\mathcal{U}, \mathcal{U})_{\mathbb{H}} = {} & (-\rho_e\zeta^2\mathbf{w}, \mathbf{u})_{\Omega_e} + (-\mathbb{C}\boldsymbol{\varepsilon}(\mathbf{w}), \boldsymbol{\varepsilon}(\mathbf{u}))_{\Omega_e} + \left(2\rho_e\zeta\mathbf{w} + \rho_e\zeta^2\mathbf{u} - \mathbf{div}\,\mathbb{C}\boldsymbol{\varepsilon}(\mathbf{u}), \mathbf{w}\right)_{\Omega_e} \\ & + (-\rho_a\boldsymbol{\nabla}\phi, \boldsymbol{\nabla}\varphi)_{\Omega_a} + (-\rho_a\triangle\varphi, \phi)_{\Omega_a}.\end{aligned}$$

Taking into account the definition (A.2) of the domain $D(A)$ and integrating by parts, we obtain

$$(A\mathcal{U}, \mathcal{U})_{\mathbb{H}} = (2\rho_e\zeta\mathbf{w}, \mathbf{w})_{\Omega_e} \geqslant 0,$$

i.e., A is monotone. It then remains to verify that, for any $\mathcal{F} \equiv (\mathbf{F}_1, \mathbf{F}_2, F_3, F_4) \in \mathbb{H}$, there is (a unique) $\mathcal{U} \in D(A)$ such that $\mathcal{U} + A\mathcal{U} = \mathcal{F}$, that is,

$$\begin{aligned} \mathbf{u} - \mathbf{w} &= \mathbf{F}_1, \\ (1+2\zeta)\mathbf{w} + \zeta^2\mathbf{u} - \rho_e^{-1}\mathbf{div}\,\mathbb{C}\boldsymbol{\varepsilon}(\mathbf{u}) &= \mathbf{F}_2, \\ \varphi - \phi &= F_3, \\ \phi - c^2\triangle\varphi &= F_4. \end{aligned} \tag{A.4}$$

The first and third equations allow to express $\mathbf{w}$ and ϕ in terms of $\mathbf{u}$ and φ, respectively; substituting these two relations in the other two equations gives

$$\begin{aligned} (\zeta+1)^2\mathbf{u} - \rho_e^{-1}\mathbf{div}\,\mathbb{C}\boldsymbol{\varepsilon}(\mathbf{u}) &= (1+2\zeta)\mathbf{F}_1 + \mathbf{F}_2, \\ \varphi - c^2\triangle\varphi &= F_3 + F_4. \end{aligned} \tag{A.5}$$

Since $\mathbf{n}_e = -\mathbf{n}_a$ on Γ_{I}, and owing to the first and third equations of (A.4) and to the transmission conditions on Γ_{I} embedded in the definition of $D(A)$, the variational formulation of the above problem reads: find $(\mathbf{u}, \varphi) \in \mathbf{H}^1_D(\Omega_e) \times H^1_D(\Omega_a)$ such that, for any $(\mathbf{v}, \psi) \in \mathbf{H}^1_D(\Omega_e) \times H^1_D(\Omega_a)$,

$$\mathscr{A}((\mathbf{u}, \varphi), (\mathbf{v}, \psi)) = \mathscr{L}(\mathbf{v}, \psi),$$

where

$$\begin{aligned} \mathscr{A}((\mathbf{u}, \varphi), (\mathbf{v}, \psi)) = {} & (\rho_e(\zeta+1)^2\mathbf{u}, \mathbf{v})_{\Omega_e} + (\mathbb{C}\boldsymbol{\varepsilon}(\mathbf{u}), \boldsymbol{\varepsilon}(\mathbf{v}))_{\Omega_e} + (\rho_a\varphi\mathbf{n}_e, \mathbf{v})_{\Gamma_{\mathrm{I}}} \\ & + (\rho_a c^{-2}\varphi, \psi)_{\Omega_a} + (\rho_a\boldsymbol{\nabla}\varphi, \boldsymbol{\nabla}\psi)_{\Omega_a} - (\rho_a\mathbf{u}\cdot\mathbf{n}_e, \psi)_{\Gamma_{\mathrm{I}}} \end{aligned}$$

and

$$\mathscr{L}(\mathbf{v}, \psi) = (\rho_e(1+2\zeta)\mathbf{F}_1 + \rho_e\mathbf{F}_2, \mathbf{v})_{\Omega_e} + (\rho_a F_3\mathbf{n}_e, \mathbf{v})_{\Gamma_{\mathrm{I}}} + (\rho_a c^{-2}(F_3 + F_4), \psi)_{\Omega_a} - (\rho_a\mathbf{F}_1\cdot\mathbf{n}_e, \psi)_{\Gamma_{\mathrm{I}}}.$$

This problem is well-posed owing to the Lax–Milgram Lemma (notice, in particular, that the bilinear form $\mathscr{A}$ is coercive since the interface contributions vanish when $\mathbf{v} = \mathbf{u}$ and $\psi = \varphi$). In addition, thanks to equations (A.5) we infer that $\mathbf{u} \in \mathbf{H}^{\triangle}_{\mathbb{C}}(\Omega_e) \cap \mathbf{H}^1_D(\Omega_e)$ and $\varphi \in H^{\triangle}(\Omega_a) \cap H^1_D(\Omega_a)$. This in turn gives $(\mathbf{w}, \phi) \in \mathbf{H}^1_D(\Omega_e) \times H^1_D(\Omega_a)$ thanks to the first and third equations of (A.4). Thus, $\mathcal{U} \in D(A)$ and the proof is complete. □

A.2. Stability of the semi-discrete formulation

Proof of Theorem 6.2. Taking $\mathbf{v}_h = \dot{\mathbf{u}}_h$ and $\psi_h = \dot{\varphi}_h$ in (16), we obtain

$$\begin{aligned} & (\rho_e\ddot{\mathbf{u}}_h, \dot{\mathbf{u}}_h)_{\Omega_e} + (2\rho_e\zeta\dot{\mathbf{u}}_h, \dot{\mathbf{u}}_h)_{\Omega_e} + (\rho_e\zeta^2\mathbf{u}_h, \dot{\mathbf{u}}_h)_{\Omega_e} + \big(\boldsymbol{\sigma}_h(\mathbf{u}_h), \boldsymbol{\varepsilon}_h(\dot{\mathbf{u}}_h)\big)_{\Omega_e} \\ & \quad - \langle\{\!\{\boldsymbol{\sigma}_h(\mathbf{u}_h)\}\!\}, [\![\dot{\mathbf{u}}_h]\!]\rangle_{\mathcal{F}_h^e} - \langle[\![\mathbf{u}_h]\!], \{\!\{\boldsymbol{\sigma}_h(\dot{\mathbf{u}}_h)\}\!\}\rangle_{\mathcal{F}_h^e} + \langle\eta[\![\mathbf{u}_h]\!], [\![\dot{\mathbf{u}}_h]\!]\rangle_{\mathcal{F}_h^e} \\ & \quad + (c^{-2}\rho_a\ddot{\varphi}_h, \dot{\varphi}_h)_{\Omega_a} + (\rho_a\boldsymbol{\nabla}_h\varphi_h, \boldsymbol{\nabla}_h\dot{\varphi}_h)_{\Omega_a} - \langle\{\!\{\rho_a\boldsymbol{\nabla}_h\varphi_h\}\!\}, [\![\dot{\varphi}_h]\!]\rangle_{\mathcal{F}_h^a} \\ & \quad - \langle\rho_a[\![\varphi_h]\!], \{\!\{\boldsymbol{\nabla}_h\dot{\varphi}_h\}\!\}\rangle_{\mathcal{F}_h^a} + \langle\chi[\![\varphi_h]\!], [\![\dot{\varphi}_h]\!]\rangle_{\mathcal{F}_h^a} = (\mathbf{f}_e, \dot{\mathbf{u}}_h)_{\Omega_e} + (\rho_a f_a, \dot{\varphi}_h)_{\Omega_a}, \end{aligned}$$

that is,

$$\frac{1}{2}\frac{\mathrm{d}}{\mathrm{d}t}\left(\|\mathbf{U}_h\|_{\mathcal{E}}^2 - 2\left(\langle\{\!\{\boldsymbol{\sigma}_h(\mathbf{u}_h)\}\!\},[\![\mathbf{u}_h]\!]\rangle_{\mathcal{F}_h^e} + \langle\{\!\{\rho_a\boldsymbol{\nabla}_h\varphi_h\}\!\},[\![\varphi_h]\!]\rangle_{\mathcal{F}_h^a}\right)\right) + 2\|\rho_e^{1/2}\zeta^{1/2}\dot{\mathbf{u}}_h\|_{\Omega_e}^2 = (\mathbf{f}_e,\dot{\mathbf{u}}_h)_{\Omega_e} + (\rho_a f_a,\dot{\varphi}_h)_{\Omega_a}.$$

Integrating the above identity over the interval $(0,t)$ we have

$$\begin{aligned}\|\mathbf{U}_h(t)\|_{\mathcal{E}}^2 - 2\left(\langle\{\!\{\boldsymbol{\sigma}_h(\mathbf{u}_h(t))\}\!\},[\![\mathbf{u}_h(t)]\!]\rangle_{\mathcal{F}_h^e} + \langle\{\!\{\rho_a\boldsymbol{\nabla}_h\varphi_h(t)\}\!\},[\![\varphi_h(t)]\!]\rangle_{\mathcal{F}_h^a}\right)\\ + 4\int_0^t \|\rho_e^{1/2}\zeta^{1/2}\dot{\mathbf{u}}_h(\tau)\|_{\Omega_e}^2\,\mathrm{d}\tau = \|\mathbf{U}_h(0)\|_{\mathcal{E}}^2 - 2\left(\langle\{\!\{\boldsymbol{\sigma}_h(\mathbf{u}_h(0))\}\!\},[\![\mathbf{u}_h(0)]\!]\rangle_{\mathcal{F}_h^e}\right.\\ \left. + \langle\{\!\{\rho_a\boldsymbol{\nabla}_h\varphi_h(0)\}\!\},[\![\varphi_h(0)]\!]\rangle_{\mathcal{F}_h^a}\right) + 2\int_0^t \big(\mathbf{f}_e(\tau),\dot{\mathbf{u}}_h(\tau)\big)_{\Omega_e}\,\mathrm{d}\tau + 2\int_0^t \big(\rho_a f_a(\tau),\dot{\varphi}_h(\tau)\big)_{\Omega_a}\,\mathrm{d}\tau,\end{aligned}$$

and, since the last term on the left-hand side is positive, we get

$$\begin{aligned}\|\mathbf{U}_h(t)\|_{\mathcal{E}}^2 - 2\left(\langle\{\!\{\boldsymbol{\sigma}_h(\mathbf{u}_h(t))\}\!\},[\![\mathbf{u}_h(t)]\!]\rangle_{\mathcal{F}_h^e} + \langle\{\!\{\rho_a\boldsymbol{\nabla}_h\varphi_h(t)\}\!\},[\![\varphi_h(t)]\!]\rangle_{\mathcal{F}_h^a}\right)\\ \leqslant \|\mathbf{U}_h(0)\|_{\mathcal{E}}^2 - 2\left(\langle\{\!\{\boldsymbol{\sigma}_h(\mathbf{u}_h(0))\}\!\},[\![\mathbf{u}_h(0)]\!]\rangle_{\mathcal{F}_h^e} + \langle\{\!\{\rho_a\boldsymbol{\nabla}_h\varphi_h(0)\}\!\},[\![\varphi_h(0)]\!]\rangle_{\mathcal{F}_h^a}\right)\\ + 2\int_0^t \big(\mathbf{f}_e(\tau),\dot{\mathbf{u}}_h(\tau)\big)_{\Omega_e}\,\mathrm{d}\tau + 2\int_0^t \big(\rho_a f_a(\tau),\dot{\varphi}_h(\tau)\big)_{\Omega_a}\,\mathrm{d}\tau.\end{aligned}$$

From Lemma A.II, we get

$$\begin{aligned}\|\mathbf{U}_h(t)\|_{\mathcal{E}}^2 - 2\left(\langle\{\!\{\boldsymbol{\sigma}_h(\mathbf{u}_h(t))\}\!\},[\![\mathbf{u}_h(t)]\!]\rangle_{\mathcal{F}_h^e} + \langle\{\!\{\rho_a\boldsymbol{\nabla}_h\varphi_h(t)\}\!\},[\![\varphi_h(t)]\!]\rangle_{\mathcal{F}_h^a}\right) &\gtrsim \|\mathbf{U}_h(t)\|_{\mathcal{E}}^2,\\ \|\mathbf{U}_h(0)\|_{\mathcal{E}}^2 - 2\left(\langle\{\!\{\boldsymbol{\sigma}_h(\mathbf{u}_h(0))\}\!\},[\![\mathbf{u}_h(0)]\!]\rangle_{\mathcal{F}_h^e} + \langle\{\!\{\rho_a\boldsymbol{\nabla}_h\varphi_h(0)\}\!\},[\![\varphi_h(0)]\!]\rangle_{\mathcal{F}_h^a}\right) &\lesssim \|\mathbf{U}_h(0)\|_{\mathcal{E}}^2,\end{aligned}$$

where the first bound holds if the stability parameters α and β are chosen large enough. Consequently

$$\begin{aligned}\|\mathbf{U}_h(t)\|_{\mathcal{E}}^2 &\lesssim \|\mathbf{U}_h(0)\|_{\mathcal{E}}^2 + 2\int_0^t \big(\mathbf{f}_e(\tau),\dot{\mathbf{u}}_h(\tau)\big)_{\Omega_e}\,\mathrm{d}\tau + 2\int_0^t \big(\rho_a f_a(\tau),\dot{\varphi}_h(\tau)\big)_{\Omega_a}\,\mathrm{d}\tau\\ &\lesssim \|\mathbf{U}_h(0)\|_{\mathcal{E}}^2 + \int_0^t \|\mathbf{f}_e(\tau)\|_{\Omega_e}\|\rho_e^{1/2}\dot{\mathbf{u}}_h(\tau)\|_{\Omega_e} + \int_0^t \|f_a(\tau)\|_{\Omega_a}\|c^{-1}\rho_a^{1/2}\dot{\varphi}_h(\tau)\|_{\Omega_a}\\ &\lesssim \|\mathbf{U}_h(0)\|_{\mathcal{E}}^2 + \int_0^t \left(\|\mathbf{f}_e(\tau)\|_{\Omega_e} + \|f_a(\tau)\|_{\Omega_a}\right)\|\mathbf{U}_h(\tau)\|_{\mathcal{E}}\,\mathrm{d}\tau,\end{aligned}$$

where we have used the Cauchy–Schwarz inequality and the definition (22) of the energy norm in the last two bounds. The assertion follows then by employing Gronwall's Lemma (see e.g. [77, p. 28]). □

A.3. Semi-discrete error estimate

Proof of Theorem 7.1. It is easy to see that the semi-discrete formulation (16) is *strongly consistent*, i.e., the exact solution $(\mathbf{u},\varphi)$ satisfies (16) for any $t\in(0,T]$:

$$\begin{aligned}(\rho_e\ddot{\mathbf{u}},\mathbf{v})_{\Omega_e}+(c^{-2}\rho_a\ddot{\varphi},\psi)_{\Omega_a}+(2\rho_e\zeta\dot{\mathbf{u}},\mathbf{v})_{\Omega_e}+(\rho_e\zeta^2\mathbf{u},\mathbf{v})_{\Omega_e}\\ +\mathcal{A}_h^e(\mathbf{u},\mathbf{v})+\mathcal{A}_h^a(\varphi,\psi)+\mathcal{I}_h^e(\dot{\varphi},\mathbf{v})+\mathcal{I}_h^a(\dot{\mathbf{u}},\psi)\\ =(\mathbf{f}_e,\mathbf{v})_{\Omega_e}+(\rho_a f_a,\psi)_{\Omega_a},\quad\forall(\mathbf{v},\psi)\in\mathbf{V}_h^e\times V_h^a.\end{aligned}\tag{A.6}$$

Subtracting (16) from the above identity, we obtain the *error equation*:

$$\begin{aligned}(\rho_e\ddot{\mathbf{e}}_e,\mathbf{v})_{\Omega_e}+(c^{-2}\rho_a\ddot{e}_a,\psi)_{\Omega_a}+(2\rho_e\zeta\dot{\mathbf{e}}_e,\mathbf{v})_{\Omega_e}+(\rho_e\zeta^2\mathbf{e}_e,\mathbf{v})_{\Omega_e}\\ +\mathcal{A}_h^e(\mathbf{e}_e,\mathbf{v})+\mathcal{A}_h^a(e_a,\psi)+\mathcal{I}_h^e(\dot{e}_a,\mathbf{v})+\mathcal{I}_h^a(\dot{\mathbf{e}}_e,\psi)=0,\quad\forall(\mathbf{v},\psi)\in\mathbf{V}_h^e\times V_h^a.\end{aligned}\tag{A.7}$$

We next decompose the error $\mathbf{E}=(\mathbf{e}_e,e_a)$ as follows: $\mathbf{E}=\mathbf{E}_I-\mathbf{E}_h$, with $\mathbf{E}_I=(\mathbf{e}_I,e_I)=(\mathbf{u}-\mathbf{u}_I,\varphi-\varphi_I)$, and $\mathbf{E}_h=(\mathbf{e}_h,e_h)=(\mathbf{u}_h-\mathbf{u}_I,\varphi_h-\varphi_I)$, $(\mathbf{u}_I,\varphi_I)\in\mathbf{V}_h^e\times V_h^a$ being the interpolants defined as in Lemma 7.1. By taking as test functions $(\mathbf{v},\psi)=(\dot{\mathbf{e}}_h,\dot{e}_h)$, the above identity reads then

$$\begin{aligned}(\rho_e\ddot{\mathbf{e}}_h,\dot{\mathbf{e}}_h)_{\Omega_e}+(c^{-2}\rho_a\ddot{e}_h,\dot{e}_h)_{\Omega_a}+(2\rho_e\zeta\dot{\mathbf{e}}_h,\dot{\mathbf{e}}_h)_{\Omega_e}+(\rho_e\zeta^2\mathbf{e}_h,\dot{\mathbf{e}}_h)_{\Omega_e}\\ +\mathcal{A}_h^e(\mathbf{e}_h,\dot{\mathbf{e}}_h)+\mathcal{A}_h^a(e_h,\dot{e}_h)+\mathcal{I}_h^e(\dot{e}_h,\dot{\mathbf{e}}_h)+\mathcal{I}_h^a(\dot{\mathbf{e}}_h,\dot{e}_h)\\ =(\rho_e\ddot{\mathbf{e}}_I,\dot{\mathbf{e}}_h)_{\Omega_e}+(c^{-2}\rho_a\ddot{e}_I,\dot{e}_h)_{\Omega_a}+(2\rho_e\zeta\dot{\mathbf{e}}_I,\dot{\mathbf{e}}_h)_{\Omega_e}+(\rho_e\zeta^2\mathbf{e}_I,\dot{\mathbf{e}}_h)_{\Omega_e}\\ +\mathcal{A}_h^e(\mathbf{e}_I,\dot{\mathbf{e}}_h)+\mathcal{A}_h^a(e_I,\dot{e}_h)+\mathcal{I}_h^e(\dot{e}_I,\dot{\mathbf{e}}_h)+\mathcal{I}_h^a(\dot{\mathbf{e}}_I,\dot{e}_h).\end{aligned}$$

Using the Cauchy–Schwarz inequality to bound the terms on the right-hand side, the above estimate can be rewritten as

$$\begin{aligned}\frac{1}{2}\frac{\mathrm{d}}{\mathrm{d}t}\Big(\|\mathbf{E}_h\|_{\mathcal{E}}^2-2\langle\{\!\{\boldsymbol{\sigma}_h(\mathbf{e}_h)\}\!\},[\![\mathbf{e}_h]\!]\rangle_{\mathcal{F}_h^e}-2\langle\{\!\{\rho_a\boldsymbol{\nabla}_h e_h\}\!\},[\![e_h]\!]\rangle_{\mathcal{F}_h^a}\Big)\\ +2\|\rho_e^{1/2}\zeta^{1/2}\dot{\mathbf{e}}_h\|_{\Omega_e}^2\leqslant\|\dot{\mathbf{e}}_I\|_{\mathcal{E}_e}\|\mathbf{e}_h\|_{\mathcal{E}_e}+\|\dot{e}_I\|_{\mathcal{E}_a}\|e_h\|_{\mathcal{E}_a}+2\|\rho_e^{1/2}\zeta^{1/2}\dot{\mathbf{e}}_I\|_{\Omega_e}\|\rho_e^{1/2}\zeta^{1/2}\dot{\mathbf{e}}_h\|_{\Omega_e}\\ +\mathcal{A}_h^e(\mathbf{e}_I,\dot{\mathbf{e}}_h)+\mathcal{A}_h^a(e_I,\dot{e}_h)+\mathcal{I}_h^e(\dot{e}_I,\dot{\mathbf{e}}_h)+\mathcal{I}_h^a(\dot{\mathbf{e}}_I,\dot{e}_h)+(\rho\zeta^2\mathbf{e}_I,\dot{\mathbf{e}}_h)_{\Omega_e}.\end{aligned}$$

This inequality can be further manipulated by observing that

$$2\|\rho_e^{1/2}\zeta^{1/2}\dot{\mathbf{e}}_I\|_{\Omega_e}\|\rho_e^{1/2}\zeta^{1/2}\dot{\mathbf{e}}_h\|_{\Omega_e}\leqslant\|\rho_e^{1/2}\zeta^{1/2}\dot{\mathbf{e}}_I\|_{\Omega_e}^2+\|\rho_e^{1/2}\zeta^{1/2}\dot{\mathbf{e}}_h\|_{\Omega_e}^2;$$

thereby we obtain

$$\begin{aligned}\frac{1}{2}\frac{\mathrm{d}}{\mathrm{d}t}\Big(\|\mathbf{E}_h\|_{\mathcal{E}}^2-2\langle\{\!\{\boldsymbol{\sigma}_h(\mathbf{e}_h)\}\!\},[\![\mathbf{e}_h]\!]\rangle_{\mathcal{F}_h^e}-2\langle\{\!\{\rho_a\boldsymbol{\nabla}_h e_h\}\!\},[\![e_h]\!]\rangle_{\mathcal{F}_h^a}\Big)\\ +\|\rho_e^{1/2}\zeta^{1/2}\dot{\mathbf{e}}_h\|_{\Omega_e}^2\leqslant\|\dot{\mathbf{e}}_I\|_{\mathcal{E}_e}\|\mathbf{e}_h\|_{\mathcal{E}_e}+\|\dot{e}_I\|_{\mathcal{E}_a}\|e_h\|_{\mathcal{E}_a}+\|\rho_e^{1/2}\zeta^{1/2}\dot{\mathbf{e}}_I\|_{\Omega_e}^2\\ +\mathcal{A}_h^e(\mathbf{e}_I,\dot{\mathbf{e}}_h)+\mathcal{A}_h^a(e_I,\dot{e}_h)+\mathcal{I}_h^e(\dot{e}_I,\dot{\mathbf{e}}_h)+\mathcal{I}_h^a(\dot{\mathbf{e}}_I,\dot{e}_h)+(\rho\zeta^2\mathbf{e}_I,\dot{\mathbf{e}}_h)_{\Omega_e}.\end{aligned}$$

Since $\|\rho_e^{1/2}\zeta^{1/2}\dot{\mathbf{e}}_h\|_{\Omega_e}^2\geqslant 0$, integrating in time between 0 and t, using Lemma A.II, and choosing the projections of the initial data such that $\mathbf{e}_h(0)=\mathbf{u}_{0,h}-(\mathbf{u}_0)_I=\mathbf{0}$ and $e_h(0)=\varphi_{0,h}-(\varphi_0)_I=0$,

we get

$$\|\mathbf{E}_h\|_{\mathcal{E}}^2 \lesssim \int_0^t (\|\dot{\mathbf{e}}_I\|_{\mathcal{E}_e}\|\mathbf{e}_h\|_{\mathcal{E}_e} + \|\dot{e}_I\|_{\mathcal{E}_a}\|e_h\|_{\mathcal{E}_a})\,\mathrm{d}\tau + \int_0^t \|\rho_e^{1/2}\zeta^{1/2}\dot{\mathbf{e}}_I\|_{\Omega_e}^2\mathrm{d}\tau + \int_0^t (\rho_e\zeta^2\mathbf{e}_I, \dot{\mathbf{e}}_h)_{\Omega_e}\mathrm{d}\tau$$
$$+ \int_0^t \big(\mathcal{A}_h^e(\mathbf{e}_I, \dot{\mathbf{e}}_h) + \mathcal{A}_h^a(e_I, \dot{e}_h)\big)\mathrm{d}\tau + \int_0^t \big(\mathcal{I}_h^e(\dot{e}_I, \dot{\mathbf{e}}_h) + \mathcal{I}_h^a(\dot{\mathbf{e}}_I, \dot{e}_h)\big)\mathrm{d}\tau. \quad \text{(A.8)}$$

Performing integration by parts in time between 0 and t on the third term on the right-hand side, and using the fact that $\mathbf{e}_h(0) = \mathbf{0}$, $e_h(0) = 0$ and the definition (22) of the energy norm yields

$$\int_0^t (\rho_e\zeta^2\mathbf{e}_I, \dot{\mathbf{e}}_h)_{\Omega_e}\mathrm{d}\tau = (\rho_e\zeta^2\mathbf{e}_I(t), \mathbf{e}_h(t))_{\Omega_e} - \int_0^t (\rho_e\zeta^2\dot{\mathbf{e}}_I, \mathbf{e}_h)_{\Omega_e}\mathrm{d}\tau$$
$$\lesssim \|\mathbf{e}_I\|_{\mathcal{E}_e}\|\mathbf{e}_h\|_{\mathcal{E}_e} + \int_0^t \|\dot{\mathbf{e}}_I\|_{\mathcal{E}_e}\|\mathbf{e}_h\|_{\mathcal{E}_e}\mathrm{d}\tau.$$

Analogously, using the continuity of bilinear forms $\mathcal{A}_h^e$ and $\mathcal{A}_h^a$ expressed by (21), and the definition (22) of the energy norm, we obtain

$$\int_0^t \big(\mathcal{A}_h^e(\mathbf{e}_I, \dot{\mathbf{e}}_h) + \mathcal{A}_h^a(e_I, \dot{e}_h)\big)\mathrm{d}\tau = \mathcal{A}_h^e(\mathbf{e}_I(t), \mathbf{e}_h(t)) + \mathcal{A}_h^a(e_I(t), e_h(t))$$
$$- \int_0^t \big(\mathcal{A}_h^e(\dot{\mathbf{e}}_I, \mathbf{e}_h) + \mathcal{A}_h^a(\dot{e}_I, e_h)\big)\mathrm{d}\tau$$
$$\lesssim |||\mathbf{e}_I|||_{\mathrm{dG},e}\|\mathbf{e}_h\|_{\mathcal{E}_e} + |||e_I|||_{\mathrm{dG},a}\|e_h\|_{\mathcal{E}_a}$$
$$+ \int_0^t \big(|||\dot{\mathbf{e}}_I|||_{\mathrm{dG},e}\|\mathbf{e}_h\|_{\mathcal{E}_e} + |||\dot{e}_I|||_{\mathrm{dG},a}\|e_h\|_{\mathcal{E}_a}\big)\mathrm{d}\tau.$$

We now seek a bound on the fifth term on the right-hand side of (A.8). Focusing on the bilinear form $\mathcal{I}_h^e$ (cf. definition (17)), we have

$$\mathcal{I}_h^e(\dot{e}_I, \dot{\mathbf{e}}_h) = \sum_{F\in\mathcal{F}_{h,\mathrm{I}}} (\rho_a\dot{e}_I\mathbf{n}_e, \dot{\mathbf{e}}_h)_F \leqslant \sum_{F\in\mathcal{F}_{h,\mathrm{I}}} \|\rho_a\dot{e}_I\|_F\|\dot{\mathbf{e}}_h\|_F \lesssim \sum_{\kappa^e\in\mathcal{T}_{h,\mathrm{I}}^e,\,\kappa^a\in\mathcal{T}_{h,\mathrm{I}}^a} \|\dot{e}_I\|_{\partial\kappa^a}\|\dot{\mathbf{e}}_h\|_{\partial\kappa^e}$$
$$\lesssim \sum_{\kappa^e\in\mathcal{T}_{h,\mathrm{I}}^e,\,\kappa^a\in\mathcal{T}_{h,\mathrm{I}}^a} p_{e,\kappa^e}h_{\kappa^e}^{-1/2}\|\dot{e}_I\|_{\partial\kappa^a}\|\dot{\mathbf{e}}_h\|_{\kappa^e}\|\mathbf{e}_h\|_{\mathcal{E}_e},$$

where we have used the Cauchy–Schwarz inequality, the trace-inverse inequality (14), the definition (22) of the energy norm, and, in the last bound, Assumption 1c on *hp*-local quasi-uniformity. Hence, we have

$$\int_0^t \mathcal{I}_h^e(\dot{e}_I, \dot{\mathbf{e}}_h)\,\mathrm{d}\tau \lesssim \int_0^t \Bigg(\sum_{\kappa\in\mathcal{T}_{h,\mathrm{I}}^a} p_{a,\kappa}h_\kappa^{-1/2}\|\dot{e}_I\|_{\partial\kappa}\Bigg)\|\mathbf{e}_h\|_{\mathcal{E}_e}\mathrm{d}\tau \overset{\mathrm{def}}{=} \int_0^t \mathcal{J}_h^a(\dot{e}_I)\|\mathbf{e}_h\|_{\mathcal{E}_e}\mathrm{d}\tau. \quad \text{(A.9)}$$

Recalling that $\mathcal{I}_h^a(\dot{\mathbf{e}}_I, \dot{e}_h) = -\mathcal{I}_h^e(\dot{e}_h, \dot{\mathbf{e}}_I)$, with completely analogous arguments we obtain

$$\int_0^t \mathcal{I}_h^a(\dot{\mathbf{e}}_I, \dot{e}_h)\,\mathrm{d}\tau \lesssim \int_0^t \Big(\sum_{\kappa\in\mathcal{T}_{h,\mathrm{I}}^e} p_{e,\kappa} h_\kappa^{-1/2} \|\dot{\mathbf{e}}_I\|_{\partial\kappa} \Big) \|e_h\|_{\mathcal{E}_a}\mathrm{d}\tau \overset{\mathrm{def}}{=} \int_0^t \mathcal{J}_h^e(\dot{\mathbf{e}}_I)\|e_h\|_{\mathcal{E}_a}\mathrm{d}\tau. \tag{A.10}$$

Substituting the above bounds into (A.8), we get

$$\begin{aligned}\|\mathbf{E}_h\|_{\mathcal{E}}^2 \lesssim \Big(\|\mathbf{e}_I\|_{\mathcal{E}_e} + |||\mathbf{e}_I|||_{\mathrm{dG},e}\Big)\|\mathbf{e}_h\|_{\mathcal{E}_e} + |||e_I|||_{\mathrm{dG},a}\|e_h\|_{\mathcal{E}_a} + \int_0^t \|\rho_e^{1/2}\zeta^{1/2}\dot{\mathbf{e}}_I\|_{\Omega_e}^2\mathrm{d}\tau \\ + \int_0^t \big(\|\dot{\mathbf{e}}_I\|_{\mathcal{E}_e} + |||\dot{\mathbf{e}}_I|||_{\mathrm{dG},e} + \mathcal{J}_h^e(\dot{e}_I)\big)\|\mathbf{e}_h\|_{\mathcal{E}_e}\mathrm{d}\tau + \int_0^t \big(\|\dot{e}_I\|_{\mathcal{E}_a} + |||\dot{e}_I|||_{\mathrm{dG},a} + \mathcal{J}_h^a(\dot{\mathbf{e}}_I)\big)\|e_h\|_{\mathcal{E}_a}\mathrm{d}\tau.\end{aligned}$$

Observe now that $\|\mathbf{e}_h\|_{\mathcal{E}_e} \leqslant \|\mathbf{E}_h\|_{\mathcal{E}}$ and $\|e_h\|_{\mathcal{E}_a} \leqslant \|\mathbf{E}_h\|_{\mathcal{E}}$. Thanks to Young's inequality we have

$$\begin{aligned}\Big(\|\mathbf{e}_I\|_{\mathcal{E}_e} + |||\mathbf{e}_I|||_{\mathrm{dG},e}\Big)\|\mathbf{e}_h\|_{\mathcal{E}_e} &\leqslant \frac{\epsilon}{2}\|\mathbf{e}_h\|_{\mathcal{E}_e}^2 + \frac{1}{2\epsilon}\Big(\|\mathbf{e}_I\|_{\mathcal{E}_e} + |||\mathbf{e}_I|||_{\mathrm{dG},e}\Big)^2 \\ &\leqslant \frac{\epsilon}{2}\|\mathbf{E}_h\|_{\mathcal{E}}^2 + \frac{1}{\epsilon}\Big(\|\mathbf{e}_I\|_{\mathcal{E}_e}^2 + |||\mathbf{e}_I|||_{\mathrm{dG},e}^2\Big), \\ |||e_I|||_{\mathrm{dG},a}\|e_h\|_{\mathcal{E}_a} &\leqslant \frac{\delta}{2}\|\mathbf{E}_h\|_{\mathcal{E}}^2 + \frac{1}{2\delta}|||e_I|||_{\mathrm{dG},a}^2.\end{aligned}$$

Choosing ϵ such that $1-\frac{1}{2}C\epsilon > 0$ and δ such that $1-\frac{1}{2}C(\delta+\epsilon) > 0$, C being the hidden constant in (A.8), we infer that

$$\begin{aligned}\|\mathbf{E}_h\|_{\mathcal{E}}^2 \lesssim \|\mathbf{e}_I\|_{\mathcal{E}_e}^2 + |||\mathbf{e}_I|||_{\mathrm{dG},e}^2 + |||e_I|||_{\mathrm{dG},a}^2 + \int_0^t \|\rho_e^{1/2}\zeta^{1/2}\dot{\mathbf{e}}_I\|_{\Omega_e}^2\mathrm{d}\tau \\ + \int_0^t \Big(\|\dot{\mathbf{e}}_I\|_{\mathcal{E}_e} + |||\dot{\mathbf{e}}_I|||_{\mathrm{dG},e} + \mathcal{J}_h^a(\dot{e}_I) + \|\dot{e}_I\|_{\mathcal{E}_a} + |||\dot{e}_I|||_{\mathrm{dG},a} + \mathcal{J}_h^e(\dot{\mathbf{e}}_I)\Big)\|\mathbf{E}_h\|_{\mathcal{E}}\,\mathrm{d}\tau.\end{aligned}$$

Upon setting

$$G = \sup_{t\in[0,T]}\Big(\|\mathbf{e}_I\|_{\mathcal{E}_e}^2 + |||\mathbf{e}_I|||_{\mathrm{dG},e}^2 + |||e_I|||_{\mathrm{dG},a}^2\Big) + \int_0^T \|\rho_e^{1/2}\zeta^{1/2}\dot{\mathbf{e}}_I\|_{\Omega_e}^2\mathrm{d}\tau,$$

and applying Gronwall's Lemma [77, p. 28] along with Jensen's inequality, we get

$$\|\mathbf{E}_h\|_{\mathcal{E}}^2 \lesssim G + \int_0^T \Big(\|\dot{\mathbf{e}}_I\|_{\mathcal{E}_e}^2 + |||\dot{\mathbf{e}}_I|||_{\mathrm{dG},e}^2 + \mathcal{J}_h^e(\dot{\mathbf{e}}_I)^2 + \|\dot{e}_I\|_{\mathcal{E}_a}^2 + |||\dot{e}_I|||_{\mathrm{dG},a}^2 + \mathcal{J}_h^a(\dot{e}_I)^2\Big)\,\mathrm{d}\tau. \tag{A.11}$$

Owing to *hp*-approximation boundary estimates [19, Lemma 33], we infer that

$$\begin{aligned}\mathcal{J}_h^a(\dot{e}_I) &\lesssim \sum_{\kappa\in\mathcal{T}_{h,\mathrm{I}}^a} \frac{h_\kappa^{\min(p_{a,\kappa}+1,n)-1}}{p_{a,\kappa}^{n-3/2}}\|\mathscr{E}\dot{\varphi}\|_{n,\mathcal{K}}, \\ \mathcal{J}_h^e(\dot{\mathbf{e}}_I) &\lesssim \sum_{\kappa\in\mathcal{T}_{h,\mathrm{I}}^e} \frac{h_\kappa^{\min(p_{e,\kappa}+1,m)-1}}{p_{e,\kappa}^{m-3/2}}\|\mathscr{E}\dot{\mathbf{u}}\|_{m,\mathcal{K}}\end{aligned}$$

(cf. (A.9) and (A.10)). Applying the bounds of Lemma 7.1 to estimate the energy- and dG-norms in the right-hand side of (A.11), observing that $\|\mathbf{E}(t)\|_{\mathcal{E}}^2 \leqslant 2(\|\mathbf{E}_h(t)\|_{\mathcal{E}}^2 + \|\mathbf{E}_I(t)\|_{\mathcal{E}}^2)$ $\forall t \in [0,T]$, applying again the bounds of Lemma 7.1 to estimate the second addend, and taking the supremum over $[0,T]$ of the resulting estimate, the thesis follows. □

Lemma A.I. *The following inequalities hold:*

$$\|\eta^{-1/2}\{\!\{\boldsymbol{\sigma}_h(\mathbf{v})\}\!\}\|_{\mathcal{F}_h^e} \lesssim \frac{1}{\sqrt{\alpha}}\|\mathbb{C}^{1/2}\boldsymbol{\varepsilon}_h(\mathbf{v})\|_{\Omega_e} \quad \forall \mathbf{v} \in \mathbf{V}_h^e, \tag{A.12a}$$

$$\|\chi^{-1/2}\{\!\{\rho_a \boldsymbol{\nabla}_h \psi\}\!\}\|_{\mathcal{F}_h^a} \lesssim \frac{1}{\sqrt{\beta}}\|\rho_a^{1/2}\boldsymbol{\nabla}_h\psi\|_{\Omega_a} \quad \forall \psi \in V_h^a, \tag{A.12b}$$

where α and β are the stability parameters appearing in the definition of stabilization functions (18a)–(18b).

Proof. We only prove (A.12a), the arguments for showing (A.12b) being completely analogous.

Recall that the following trace-inverse inequality holds for simplices [19, p. 25]: given a simplex $T \subset \mathbb{R}^d$ and a polynomial degree $p \geqslant 1$, for all $v \in \mathscr{P}_p(T)$ there is a real number $C > 0$ independent of the discretization parameters such that

$$\|v\|_F^2 \leqslant Cp^2\frac{|F|}{|T|}\|v\|_T^2. \tag{A.13}$$

Owing to (A.13), the definition (9) of $\overline{\mathbb{C}}_\kappa$, the definition (18a) of η, and Assumption 1a, for any $\mathbf{v} \in \mathbf{V}_h^e$ we obtain

$$\begin{aligned}\|\eta^{-1/2}\{\!\{\boldsymbol{\sigma}_h(\mathbf{v})\}\!\}\|_{\mathcal{F}_h^e}^2 &\leqslant \sum_{\kappa\in\mathcal{T}_h^e}\sum_{F\subset\partial\kappa}\overline{\mathbb{C}}_\kappa\|\eta^{-1/2}\mathbb{C}^{1/2}\boldsymbol{\varepsilon}(\mathbf{v})\|_F^2\\ &\lesssim \sum_{\kappa\in\mathcal{T}_h^e}\sum_{F\subset\partial\kappa}\eta^{-1}\overline{\mathbb{C}}_\kappa p_{e,\kappa}^2\frac{|F|}{|\kappa_\flat^F|}\|\mathbb{C}^{1/2}\boldsymbol{\varepsilon}(\mathbf{v})\|_{\kappa_\flat^F}^2 \lesssim \frac{1}{\alpha}\|\mathbb{C}^{1/2}\boldsymbol{\varepsilon}_h(\mathbf{v})\|_{\Omega_e}^2.\end{aligned}$$

□

Lemma A.II. *For any $\mathbf{W} = (\mathbf{v},\psi) \in C^1([0,T];\mathbf{V}_h^e)\times C^1([0,T];V_h^a)$, it holds*

$$\begin{aligned}\|\mathbf{W}\|_{\mathcal{E}}^2 - 2\left(\langle\{\!\{\boldsymbol{\sigma}_h(\mathbf{v})\}\!\},[\![\mathbf{v}]\!]\rangle_{\mathcal{F}_h^e} + \langle\{\!\{\rho_a\boldsymbol{\nabla}_h\psi\}\!\},[\![\psi]\!]\rangle_{\mathcal{F}_h^a}\right) &\lesssim \|\mathbf{W}\|_{\mathcal{E}}^2,\\ \|\mathbf{W}\|_{\mathcal{E}}^2 - 2\left(\langle\{\!\{\boldsymbol{\sigma}_h(\mathbf{v})\}\!\},[\![\mathbf{v}]\!]\rangle_{\mathcal{F}_h^e} + \langle\{\!\{\rho_a\boldsymbol{\nabla}_h\psi\}\!\},[\![\psi]\!]\rangle_{\mathcal{F}_h^a}\right) &\gtrsim \|\mathbf{W}\|_{\mathcal{E}}^2,\end{aligned} \tag{A.14}$$

Proof. The first bound follows from the Cauchy–Schwarz inequality, the definition (22) of the energy norm, and Lemma A.I:

$$\begin{aligned}&\|\mathbf{W}\|_{\mathcal{E}}^2 - 2\left(\langle\{\!\{\boldsymbol{\sigma}_h(\mathbf{v})\}\!\},[\![\mathbf{v}]\!]\rangle_{\mathcal{F}_h^e} + \langle\{\!\{\rho_a\boldsymbol{\nabla}_h\psi\}\!\},[\![\psi]\!]\rangle_{\mathcal{F}_h^a}\right)\\ &\quad\lesssim \|\mathbf{W}\|_{\mathcal{E}}^2 + \|\eta^{-1/2}\{\!\{\boldsymbol{\sigma}_h(\mathbf{v})\}\!\}\|_{\mathcal{F}_h^e}\|\eta^{1/2}[\![\mathbf{v}]\!]\|_{\mathcal{F}_h^e} + \|\chi^{-1/2}\{\!\{\rho_a\boldsymbol{\nabla}_h\psi\}\!\}\|_{\mathcal{F}_h^a}\|\chi^{1/2}[\![\psi]\!]\|_{\mathcal{F}_h^a}\\ &\quad\lesssim \|\mathbf{W}\|_{\mathcal{E}}^2 + \frac{1}{\sqrt{\alpha}}\|\mathbb{C}^{1/2}\boldsymbol{\varepsilon}_h(\mathbf{v})\|_{\Omega_e}\|\mathbf{v}\|_{\mathrm{dG},e} + \frac{1}{\sqrt{\beta}}\|\rho_a^{1/2}\boldsymbol{\nabla}_h\psi\|_{\Omega_a}\|\psi\|_{\mathrm{dG},a}\end{aligned}$$

$$\lesssim \|\mathbf{W}\|_{\mathcal{E}}^2 + \|\mathbf{W}\|_{\mathrm{dG}}^2 \lesssim \|\mathbf{W}\|_{\mathcal{E}}^2,$$

where we have set $\|\mathbf{W}\|_{\mathrm{dG}}^2 = \|\mathbf{v}\|_{\mathrm{dG},e}^2 + \|\psi\|_{\mathrm{dG},a}^2$. To prove the second bound, it suffices to show that

$$\|\mathbf{W}\|_{\mathrm{dG}}^2 - 2\left(\langle\{\!\{\boldsymbol{\sigma}_h(\mathbf{v})\}\!\}, [\![\mathbf{v}]\!]\rangle_{\mathcal{F}_h^e} + \langle\{\!\{\rho_a \boldsymbol{\nabla}_h \psi\}\!\}, [\![\psi]\!]\rangle_{\mathcal{F}_h^a}\right) \gtrsim \|\mathbf{W}\|_{\mathrm{dG}}^2. \tag{A.15}$$

Indeed, by the definition (22) of the energy norm and (A.15),

$$\begin{aligned}
&\|\mathbf{W}\|_{\mathcal{E}}^2 - 2\left(\langle\{\!\{\boldsymbol{\sigma}_h(\mathbf{v})\}\!\}, [\![\mathbf{v}]\!]\rangle_{\mathcal{F}_h^e} + \langle\{\!\{\rho_a \boldsymbol{\nabla}_h \psi\}\!\}, [\![\psi]\!]\rangle_{\mathcal{F}_h^a}\right) \\
&= \|\rho_e^{1/2}\dot{\mathbf{v}}\|_{\Omega_e}^2 + \|\rho_e^{1/2}\zeta\mathbf{v}\|_{\Omega_e}^2 + \|c^{-1}\rho_a^{1/2}\dot{\psi}\|_{\Omega_a}^2 + \|\mathbf{W}\|_{\mathrm{dG}}^2 - 2\left(\langle\{\!\{\boldsymbol{\sigma}_h(\mathbf{v})\}\!\}, [\![\mathbf{v}]\!]\rangle_{\mathcal{F}_h^e} + \langle\{\!\{\rho_a \boldsymbol{\nabla}_h \psi\}\!\}, [\![\psi]\!]\rangle_{\mathcal{F}_h^a}\right) \\
&\gtrsim \|\rho_e^{1/2}\dot{\mathbf{v}}\|_{\Omega_e}^2 + \|\rho_e^{1/2}\zeta\mathbf{v}\|_{\Omega_e}^2 + \|c^{-1}\rho_a^{1/2}\dot{\psi}\|_{\Omega_a}^2 + \|\mathbf{W}\|_{\mathrm{dG}}^2 = \|\mathbf{W}\|_{\mathcal{E}}^2.
\end{aligned}$$

Thus, we next show that (A.15) holds provided the stability parameters α and β are chosen large enough. To this purpose, using Young's inequality we infer that, for any $\delta, \epsilon > 0$,

$$\begin{aligned}
\langle\{\!\{\boldsymbol{\sigma}_h(\mathbf{v})\}\!\}, [\![\mathbf{v}]\!]\rangle_{\mathcal{F}_h^e} &\leqslant \sum_{F\in\mathcal{F}_h^e} \|\eta^{-1/2}\{\!\{\boldsymbol{\sigma}_h(\mathbf{v})\}\!\}\|_F \|\eta^{1/2}[\![\mathbf{v}]\!]\|_F \leqslant \frac{1}{2\delta}\|\eta^{-1/2}\{\!\{\boldsymbol{\sigma}_h(\mathbf{v})\}\!\}\|_{\mathcal{F}_h^e}^2 + \frac{\delta}{2}\|\eta^{1/2}[\![\mathbf{v}]\!]\|_{\mathcal{F}_h^e}^2, \\
\langle\{\!\{\rho_a \boldsymbol{\nabla}_h \psi\}\!\}, [\![\psi]\!]\rangle_{\mathcal{F}_h^a} &\leqslant \sum_{F\in\mathcal{F}_h^a} \|\chi^{-1/2}\{\!\{\rho_a \boldsymbol{\nabla}_h \psi\}\!\}\|_F \|\chi^{1/2}[\![\psi]\!]\|_F \leqslant \frac{1}{2\epsilon}\|\chi^{-1/2}\{\!\{\rho_a \boldsymbol{\nabla}_h \psi\}\!\}\|_{\mathcal{F}_h^a}^2 + \frac{\epsilon}{2}\|\chi^{1/2}[\![\psi]\!]\|_{\mathcal{F}_h^a}^2.
\end{aligned}$$

Hence, from the definition of the $\|\cdot\|_{\mathrm{dG},e}$- and $\|\cdot\|_{\mathrm{dG},a}$-norms on $\mathbf{V}_h^e$ and V_h^a, it follows that

$$\begin{aligned}
&\|\mathbf{W}\|_{\mathrm{dG}}^2 - 2\left(\langle\{\!\{\boldsymbol{\sigma}_h(\mathbf{v})\}\!\}, [\![\mathbf{v}]\!]\rangle_{\mathcal{F}_h^e} + \langle\{\!\{\rho_a \boldsymbol{\nabla}_h \psi\}\!\}, [\![\psi]\!]\rangle_{\mathcal{F}_h^a}\right) \\
&\qquad \geqslant \|\mathbb{C}^{1/2}\boldsymbol{\varepsilon}(\mathbf{v})\|_{\Omega_e}^2 + \|\rho_a^{1/2}\boldsymbol{\nabla}_h\psi\|_{\Omega_a}^2 + (1-\delta)\,\|\eta^{1/2}[\![\mathbf{v}]\!]\|_{\mathcal{F}_h^e}^2 - \frac{1}{\delta}\|\eta^{-1/2}\{\!\{\boldsymbol{\sigma}_h(\mathbf{v})\}\!\}\|_{\mathcal{F}_h^e}^2 \\
&\qquad\qquad + (1-\epsilon)\,\|\chi^{1/2}[\![\psi]\!]\|_{\mathcal{F}_h^a}^2 - \frac{1}{\epsilon}\|\chi^{-1/2}\{\!\{\rho_a \boldsymbol{\nabla}_h \psi\}\!\}\|_{\mathcal{F}_h^a}^2 \\
&\qquad \geqslant \left(1 - \frac{C_1}{\alpha\delta}\right)\|\mathbb{C}^{1/2}\boldsymbol{\varepsilon}_h(\mathbf{v})\|_{\Omega_e}^2 + \left(1 - \frac{C_2}{\beta\epsilon}\right)\|\rho_a^{1/2}\boldsymbol{\nabla}_h\psi\|_{\Omega_a}^2 \\
&\qquad\qquad + (1-\delta)\,\|\eta^{1/2}[\![\mathbf{v}]\!]\|_{\mathcal{F}_h^e}^2 + (1-\epsilon)\,\|\chi^{1/2}[\![\psi]\!]\|_{\mathcal{F}_h^a}^2,
\end{aligned}$$

where in the last bound we have applied Lemma A.I with hidden constants C_1 and C_2. Then (A.15) follows by choosing, for instance, $\delta = \epsilon = 1/2$ and $\alpha \geqslant 4C_1$, $\beta \geqslant 4C_2$. □

References

References

[1] D. N. Arnold, F. Brezzi, B. Cockburn, L. D. Marini, Unified analysis of discontinuous Galerkin methods for elliptic problems, SIAM J. Numer. Anal. 39 (2002) 1749–1779.

[2] B. Rivière, Discontinuous Galerkin methods for solving elliptic and parabolic equations, Frontiers in Applied Mathematics, SIAM, 2008.

[3] D. A. Di Pietro, A. Ern, Mathematical aspects of Discontinuous Galerkin methods, Mathématiques & Applications, Springer-Verlag, 2012.

[4] J. S. Hesthaven, T. Warburton, Nodal Discontinuous Galerkin Methods, Vol. 54 of Texts in Applied Mathematics, Springer-Verlag New York, 2008.

[5] S. Esterhazy, F. Schneider, I. Mazzieri, G. Bokelmann, Insights into the modeling of seismic waves for the detection of underground cavities, Tech. Rep. 67/2017, MOX, Politecnico di Milano (2017).

[6] S. Esterhazy, F. Schneider, I. Perugia, G. Bokelmann, Application of high-order finite-element method to the p-wave propagation around and inside an underground cavity, Geophysics 82 (2017) T197–T206.

[7] F. Schneider, S. Esterhazy, I. Perugia, G. Bokelmann, Seismic resonances of spherical acoustic cavities, Geophysical Prospecting 65 (2017) 1–24.

[8] B. Flemisch, M. Kaltenbacher, B. I. Wohlmuth, Elasto–acoustic and acoustic–acoustic coupling on non-matching grids, Int. J. Numer. Meth. Engng 67 (2006) 1791–1810.

[9] S. Mönköla, Numerical simulation of fluid-structure interaction between acoustic and elastic waves, Ph.D. thesis, University of Jyväskylä (2011).

[10] P. F. Antonietti, P. Houston, X. Hu, M. Sarti, M. Verani, Multigrid algorithms for *hp*-version interior penalty discontinuous Galerkin methods on polygonal and polyhedral meshes, Calcolo 54 (2017) 1169–1198.

[11] P. F. Antonietti, A. Cangiani, J. Collis, Z. Dong, E. H. Georgoulis, S. Giani, P. Houston, Review of discontinuous Galerkin finite element methods for partial differential equations on complicated domains, in: G. Barrenechea, F. Brezzi, A. Cangiani, E. Georgoulis (Eds.), Building bridges: connections and challenges in modern approaches to numerical partial differential equations, Vol. 114 of Lecture Notes in Computational Science and Engineering, Springer, Cham, 2016.

[12] P. F. Antonietti, I. Mazzieri, High-order discontinuous Galerkin methods for the elastodynamics equation on polygonal and polyhedral meshes, Comput. Methods Appl. Mech. Engrg. 342 (2018) 414–437.

[13] P. F. Antonietti, F. Brezzi, L. D. Marini, Bubble stabilization of discontinuous Galerkin methods, Comput. Methods Appl. Mech. Engrg. 198 (2009) 1651–1659.

[14] A. Cangiani, E. H. Georgoulis, P. Houston, *hp*-Version discontinuous Galerkin methods on polygonal and polyhedral meshes, Math. Models Methods Appl. Sci. 24 (2014) 2009–2041.

[15] A. Cangiani, Z. Dong, E. H. Georgoulis, P. Houston, *hp*-Version discontinuous Galerkin methods for advection–diffusion–reaction problems on polytopic meshes, ESAIM Math. Model. Numer. Anal. 50 (2016) 699–725.

[16] A. Cangiani, Z. Dong, E. H. Georgoulis, *hp*-Version space-time discontinuous Galerkin methods for parabolic problems on prismatic meshes, SIAM J. Sci. Comput. 39 (2017) A1251–A1279.

[17] P. F. Antonietti, G. Pennesi, *V*-cycle multigrid algorithms for discontinuous Galerkin methods on non-nested polytopic meshes, J. Sci. Comput. Published online. doi:10.1007/s10915-018-0783-x.

[18] P. F. Antonietti, P. Houston, G. Pennesi, Fast numerical integration on polytopic meshes with applications to discontinuous Galerkin finite element methods, J. Sci. Comput. 77 (2018) 1339–1370.

[19] A. Cangiani, Z. Dong, E. H. Georgoulis, P. Houston, *hp*-Version discontinuous Galerkin methods on polygonal and polyhedral meshes, SpringerBriefs in Mathematics, Springer International Publishing, 2017.

[20] N. Sukumar, A. Tabarrei, Conforming polygonal finite elements, Int. J. Numer. Meth. Engng 61 (2004) 2045–2066.

[21] A. Tabarrei, N. Sukumar, Application of polygonal finite elements in linear elasticity, Int. J. Comput. Methods 3 (2006) 503–520.

[22] G. Manzini, A. Russo, N. Sukumar, New perspectives on polygonal and polyhedral finite element methods, Math. Models Methods Appl. Sci. 24 (2014) 1665–1699.

[23] A. Tabarrei, N. Sukumar, Extended finite-element method on polygonal and quadtree meshes, Comput. Methods Appl. Mech. Engrg. 197 (2008) 425–438.

[24] P. F. Antonietti, N. Bigoni, M. Verani, Mimetic discretizations of elliptic control problems, J. Sci. Comput. 56 (2013) 14–27.

[25] P. F. Antonietti, L. Beirão da Veiga, M. Verani, A mimetic discretization of elliptic obstacle problems, Math. Comp. 82 (2013) 1379–1400.

[26] F. Brezzi, A. Buffa, K. Lipnikov, Mimetic finite differences for elliptic problems, ESAIM Math. Model. Numer. Anal. 43 (2009) 277–295.

[27] V. Gyrya, K. Lipnikov, G. Manzini, The arbitrary order mixed mimetic finite difference method for the diffusion equation, ESAIM Math. Model. Numer. Anal. 50 (2016) 851–877.

[28] L. Beirão da Veiga, K. Lipnikov, G. Manzini, Arbitrary-order nodal mimetic discretizations of elliptic problems on polygonal meshes, SIAM J. Numer. Anal. 49 (2011) 1737–1760.

[29] L. Beirão da Veiga, F. Brezzi, L. D. Marini, A. Russo, Basic principles of virtual element methods, Math. Models Methods Appl. Sci. 23 (2013) 199–214.

[30] L. Beirão da Veiga, F. Brezzi, L. D. Marini, A. Russo, Mixed virtual element methods for general second order elliptic problems on polygonal meshes, ESAIM Math. Model. Numer. Anal. 50 (2016) 727–747.

[31] L. Beirão da Veiga, F. Brezzi, L. D. Marini, A. Russo, Virtual element method for general second-order elliptic problems on polygonal meshes, Math. Models Methods Appl. Sci. 26 (2016) 729–750.

[32] P. F. Antonietti, M. Bruggi, S. Scacchi, M. Verani, On the virtual element method for topology optimization on polygonal meshes: A numerical study, Comput. Math. Appl. 74 (2017) 1091–1109.

[33] P. F. Antonietti, G. Manzini, M. Verani, The fully nonconforming virtual element method for biharmonic problems, Math. Models Methods Appl. Sci. 28 (2018) 387–407.

[34] B. Cockburn, J. Gopalakrishnan, R. Lazarov, Unified hybridization of discontinuous Galerkin, mixed, and continuous Galerkin methods for second order elliptic problems, SIAM J. Numer. Anal. 47 (2009) 1319–1365.

[35] R. M. Kirby, S. J. Sherwin, B. Cockburn, To CG or to HDG: a comparative study, J. Sci. Comput. 51 (2012) 183–212.

[36] B. Cockburn, J. Gopalakrishnan, F. J. Sayas, A projection-based error analysis of hdg methods, Math. Comp. 79 (2010) 1351–1367.

[37] D. A. Di Pietro, A. Ern, S. Lemaire, An arbitrary-order and compact-stencil discretization of diffusion on general meshes based on local reconstruction operators, Comput. Method Appl. Math. 14 (2014) 461–472.

[38] D. A. Di Pietro, J. Droniou, A hybrid high-order method for Leray–Lions elliptic equations on general meshes, Math. Comp. 86 (2017) 2159–2191.

[39] F. Bonaldi, D. A. Di Pietro, G. Geymonat, F. Krasucki, A hybrid high-order method for Kirchhoff–Love plate bending problems, ESAIM Math. Model. Numer. Anal. 52 (2018) 393–421.

[40] A. Bermúdez, L. Hervella-Nieto, R. Rodríguez, Finite element computation of three-dimensional elastoacoustic vibrations, Journal of Sound and Vibration 219 (1999) 279–306.

[41] H. Barucq, R. Djellouli, E. Estecahandy, Characterization of the Fréchet derivative of the elasto-acoustic field with respect to Lipschitz domains, J. Inverse Ill-Posed Probl. 22 (2014) 1–8.

[42] H. Barucq, R. Djellouli, E. Estecahandy, Efficient dg-like formulation equipped with curved boundary edges for solving elasto-acoustic scattering problems, Int. J. Numer. Meth. Engng 98 (2014) 747–780.

[43] D. Brunner, M. Junge, L. Gaul, A comparison of FE–BE coupling schemes for large-scale problems with fluid-structure interaction, Int. J. Numer. Meth. Engng 77 (2009) 664–688.

[44] J. D. De Basabe, M. K. Sen, A comparison of finite-difference and spectral-element methods for elastic wave propagation in media with a fluid-solid interface, Geophysical Journal International 200 (2015) 278–298.

[45] M. Fischer, L. Gaul, Fast BEM–FEM mortar coupling for acoustic-structure interaction, Int. J. Numer. Meth. Engng 62 (2005) 1677–1690.

[46] J. Mandel, An iterative substructuring method for coupled fluid–solid acoustic problems, J. Comput. Phys. 177 (2002) 95–116.

[47] S. Mönköla, On the accuracy and efficiency of transient spectral element models for seismic wave problems, Adv. Math. Phys. (2016) 1–15.

[48] V. Péron, Equivalent boundary conditions for an elasto-acoustic problem set in a domain with a thin layer, ESAIM Math. Model. Numer. Anal. 48 (2014) 1431–1449.

[49] L. C. Wilcox, G. Stadler, C. Burstedde, O. Ghattas, A high-order discontinuous galerkin method for wave propagation through coupled elastic-acoustic media, J. Comput. Phys. 229 (2010) 9373–9396.

[50] M. Popa, Finite element solution of scattering in coupled fluid-solid systems, Ph.D. thesis, University of Colorado (2002).

[51] G. W. Benthien, H. A. Schenck, Structural-acoustic coupling, in: R. Ciskowski, C. Brebbia (Eds.), Boundary element methods in acoustics, Computational mechanics publications, Elsevier Applied Science, Southampton, 1991.

[52] B. Flemisch, M. Kaltenbacher, S. Triebenbacher, B. I. Wohlmuth, The equivalence of standard and mixed finite element methods in applications to elasto-acoustic interaction, SIAM J. Sci. Comput. 32 (2010) 1980–2006.

[53] G. C. Hsiao, N. Nigam, A transmission problem for fluid-structure interaction in the exterior of a thin domain, Adv. Differential Equations 8 (2003) 1281–1318.

[54] G. C. Hsiao, F. J. Sayas, R. J. Weinacht, Time-dependent fluid-structure interaction, Math. Methods Appl. Sci. 40 (2017) 486–500.

[55] G. C. Hsiao, T. Sánchez-Vizuet, F. J. Sayas, Boundary and coupled boundary–finite element methods for transient wave–structure interaction, IMA J. Numer. Anal. 37 (2017) 237–265.

[56] R. A. Jeans, I. C. Mathews, Solution of fluid-structure interaction problems using a coupled finite element and variational boundary element technique, The Journal of the Acoustical Society of America 88.

[57] D. Komatitsch, C. Barnes, J. Tromp, Wave propagation near a fluid-solid interface: a spectral-element approach, Geophysics 65 (2000) 623–631.

[58] H. Y. Lee, S. C. Lim, D. J. Min, B. D. Kwon, M. Park, 2D time-domain acoustic-elastic coupled modeling: a cell-based finite-difference method, Geosciences Journal 13 (2009) 407–414.

[59] H. Brezis, Functional analysis, Sobolev spaces and partial differential equations, Universitext, Springer-Verlag New York, 2011.

[60] T. S. Brown, T. Sánchez-Vizuet, F. J. Sayas, Evolution of a semidiscrete system modeling the scattering of acoustic waves by a piezoelectric solid, ESAIM Math. Model. Numer. Anal. 52 (2018) 423–455.

[61] B. Rivière, S. Shaw, M. Wheeler, J. Whiteman, Discontinuous Galerkin finite element methods for linear elasticity and quasistatic linear viscoelasticity, Numer. Math. 95 (2003) 347–376.

[62] B. Rivière, S. Shaw, J. Whiteman, Discontinuous Galerkin finite element methods for dynamic linear solid viscoelasticity problems, Numer. Methods Partial Differential Equations 23 (2007) 1149–1166.

[63] A. Ferroni, Discontinuous Galerkin Spectral Element methods for the elastodynamics equation on hybrid hexahedral-tetrahedral grids, Ph.D. thesis, Politecnico di Milano (2017).

[64] F. Bonaldi, G. Geymonat, F. Krasucki, Modeling of smart materials with thermal effects: dynamic and quasi-static evolution, Math. Models Methods Appl. Sci. 25 (2015) 2633–2667.

[65] I. Perugia, D. Schötzau, An *hp*-analysis of the local discontinuous Galerkin method for diffusion problems, J. Sci. Comput. 17 (2002) 561–571.

[66] V. Girault, P. A. Raviart, Finite element methods for Navier-Stokes equations, Springer-Verlag New York, 1986.

[67] F. Brezzi, M. Fortin, Mixed and hybrid finite element methods, Springer Series in Computational Mathematics, Springer-Verlag New York, 1991.

[68] P. F. Antonietti, A. Ferroni, I. Mazzieri, R. Paolucci, A. Quarteroni, C. Smerzini, M. Stupazzini, Numerical modeling of seismic waves by discontinuous spectral element methods, ESAIM:ProcS 61 (2018) 1–37.

[69] A. Lozinski, A primal discontinuous Galerkin method with static condensation on very general meshes, Preprint arXiv:1803.06846, submitted (March 2018).

[70] D. N. Arnold, F. Brezzi, R. S. Falk, L. D. Marini, Locking-free Reissner–Mindlin elements without reduced integration, Comput. Methods Appl. Mech. Engrg. 196 (2007) 3660–3671.

[71] P. F. Antonietti, B. Ayuso de Dios, I. Mazzieri, A. Quarteroni, Stability analysis of discontinuous Galerkin approximations to the elastodynamics problem, J. Sci. Comput. 68 (2016) 143–170.

[72] P. F. Antonietti, A. Ferroni, I. Mazzieri, A. Quarteroni, *hp*-Version discontinuous Galerkin approximations of the elastodynamics equation, in: M. Bittencourt, N. Dumont, J. Hesthaven (Eds.), Spectral and High Order Methods for Partial Differential Equations ICOSAHOM 2016, Vol. 119 of Lecture Notes in Computational Science and Engineering, Springer, Cham, 2017.

[73] A. Quarteroni, A. Valli, Numerical Approximation of Partial Differential Equations, Vol. 23, Springer Science & Business Media, 2008.

[74] C. Talischi, G. H. Paulino, A. Pereira, I. F. M. Menezes, PolyMesher: a general-purpose mesh generator for polygonal elements written in Matlab, Struct. Multidisc. Optim. 45 (2012) 309–328.

[75] P. Antonietti, I. Mazzieri, N. Dal Santo, A. Quarteroni, A high-order discontinuous Galerkin approximation to ordinary differential equations with applications to elastodynamics, IMA Journal of Numerical Analysis 38 (4) (2018) 1709–1734.

[76] N. Ricker, The form and laws of propagation of seismic wavelets, Geophysics 18 (1953) 10–40.

[77] A. Quarteroni, Numerical Models for Differential Problems, 2nd Edition, Vol. 8 of MS&A, Springer-Verlag Mailand, 2014.